Supporting Information for:

Spin-state Tuning at Pseudotetrahedral d^6 Ions – Spin-Crossover in $[BP_3]Fe^{II}$-X Complexes

Sidney E. Creutz and Jonas C. Peters

Division of Chemistry and Chemical Engineering, California Institute of Technology, Pasadena, California 91125, United States

I. Spectroscopic characterization of complexes 1-9

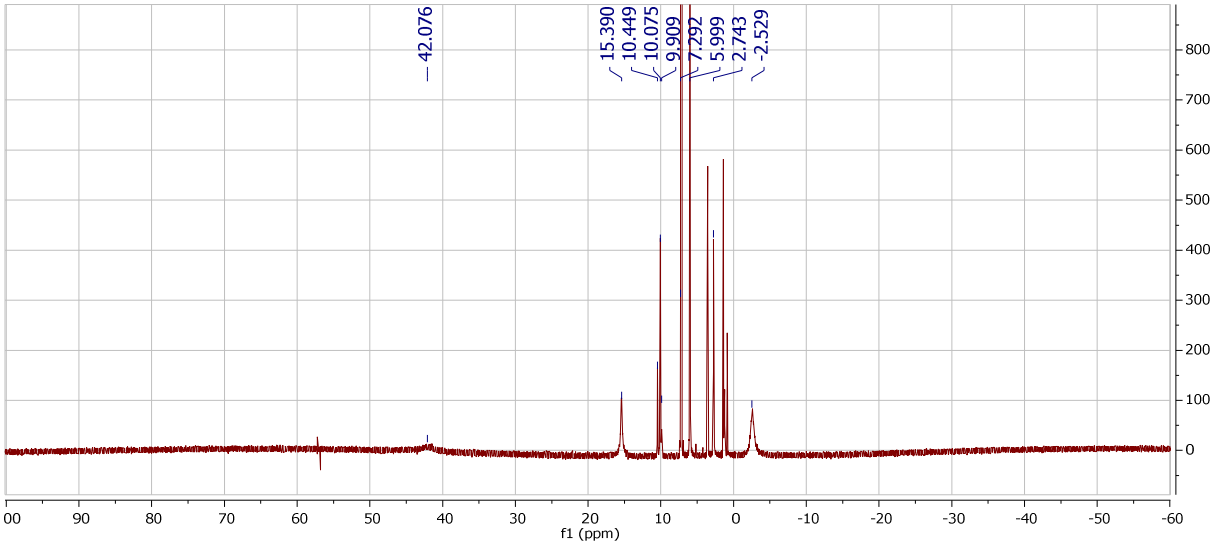

Figure S1. ^{1}H NMR spectrum of **1** in C_6D_6 (300 MHz, 298 K)

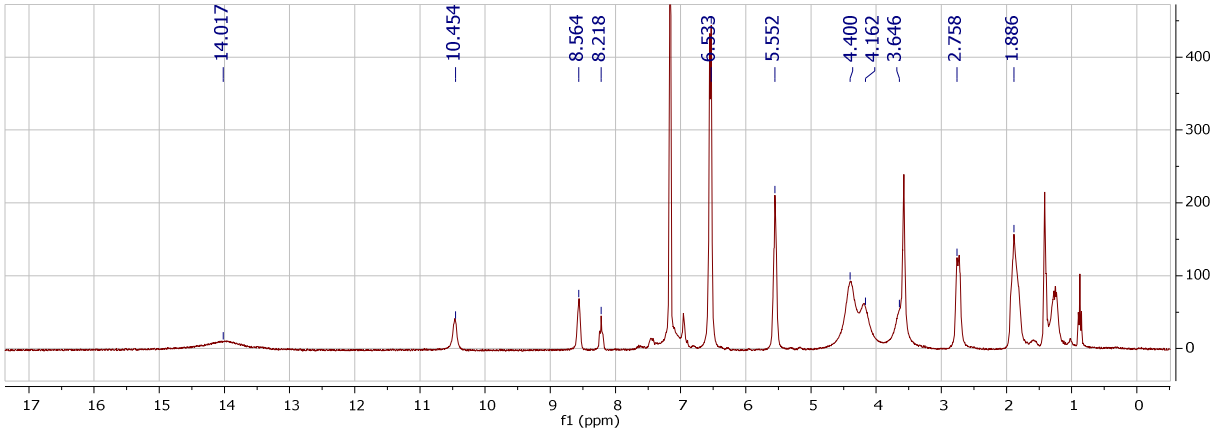

Figure S2. ^{1}H NMR spectrum of **2** in C_6D_6 (300 MHz, 298 K)

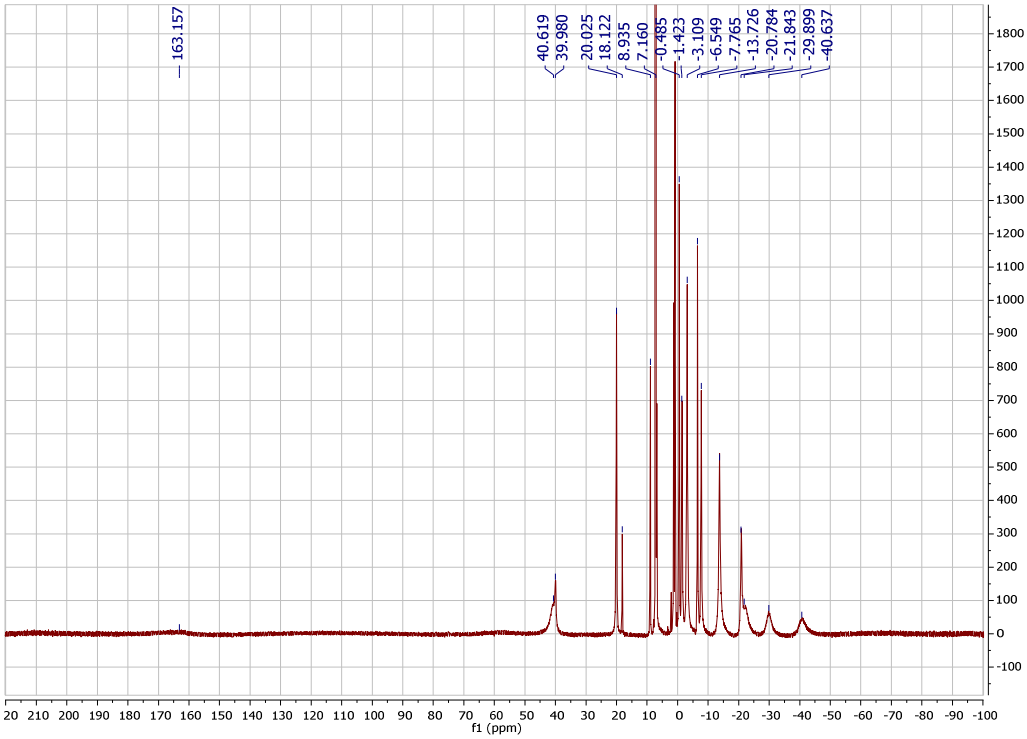

Figure S3. ^{1}H NMR of **3** in C_6D_6 (300 MHz, 298 K)

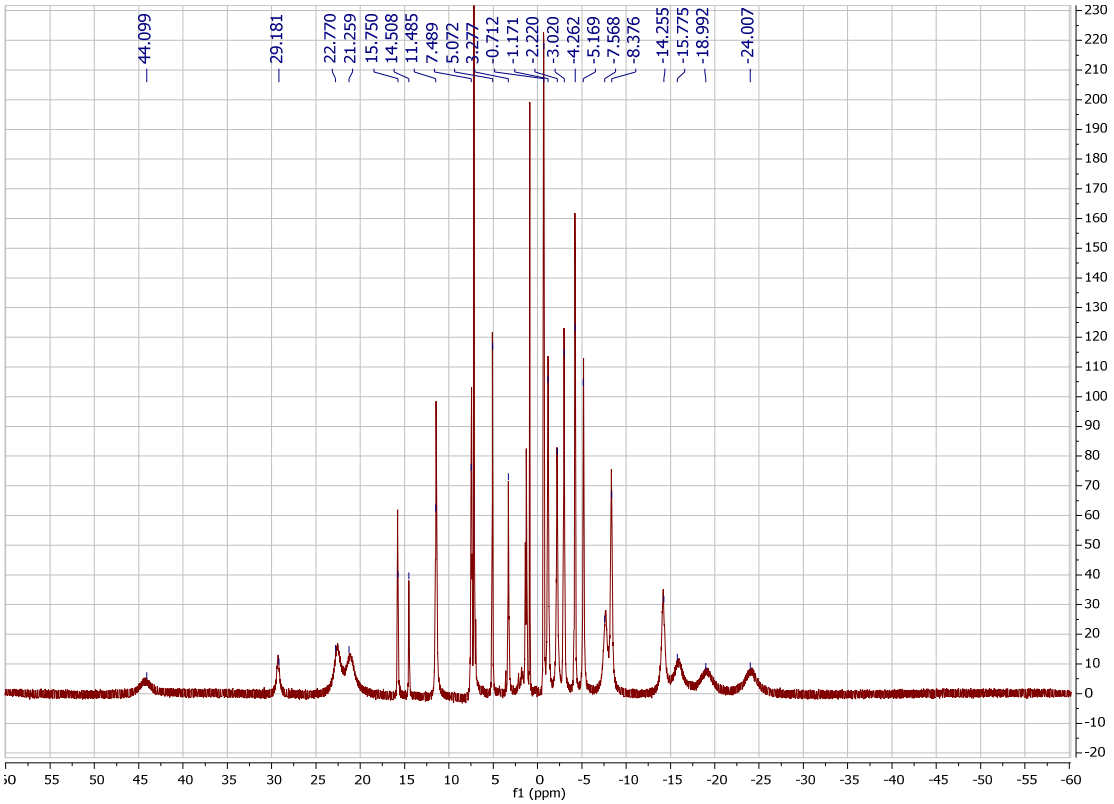

Figure S4. ^{1}H NMR spectrum of **4** in C_6D_6 (300 MHz, 298 K)

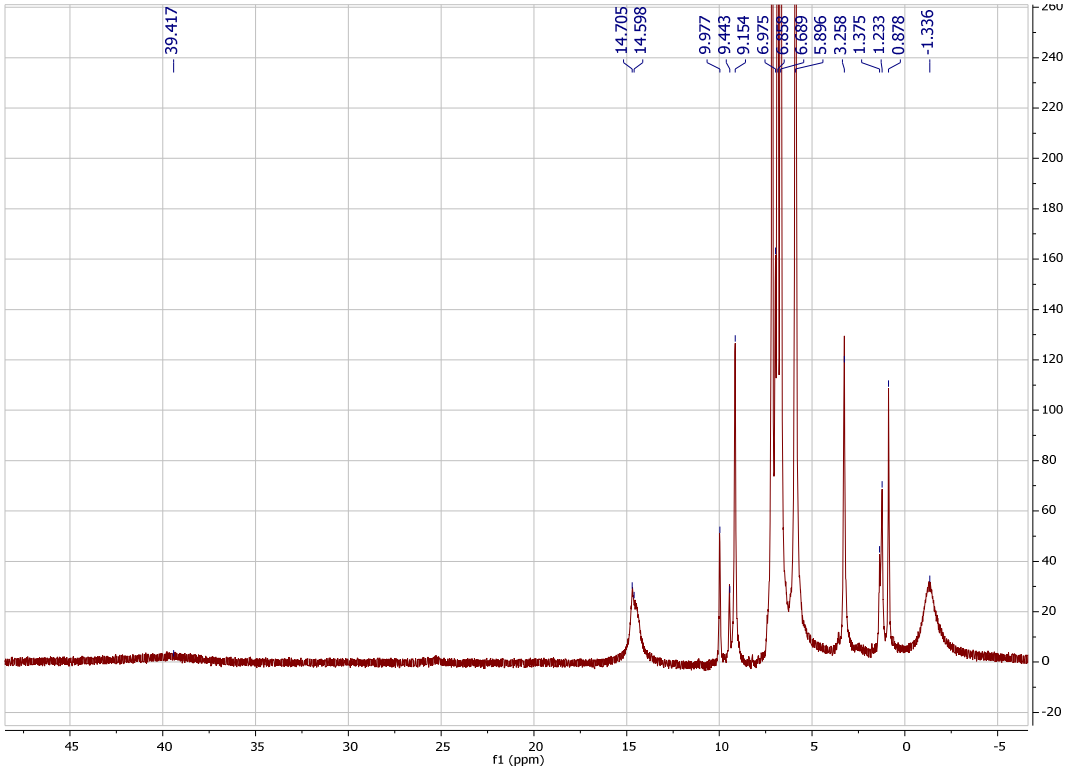

Figure S5. ^{1}H NMR of **5** in C_6D_6 (300 MHz, 298 K)

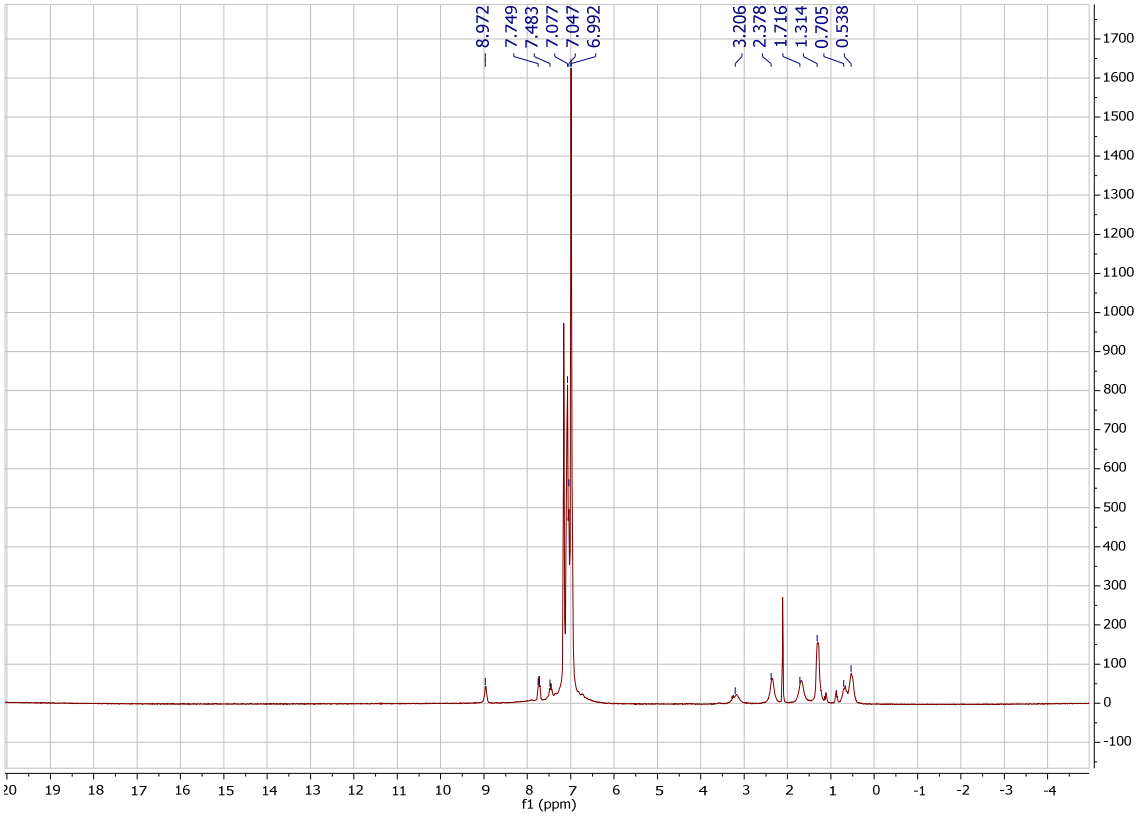

Figure S6. ^{1}H NMR of **6** in C_6D_6 (300 MHz, 298 K)

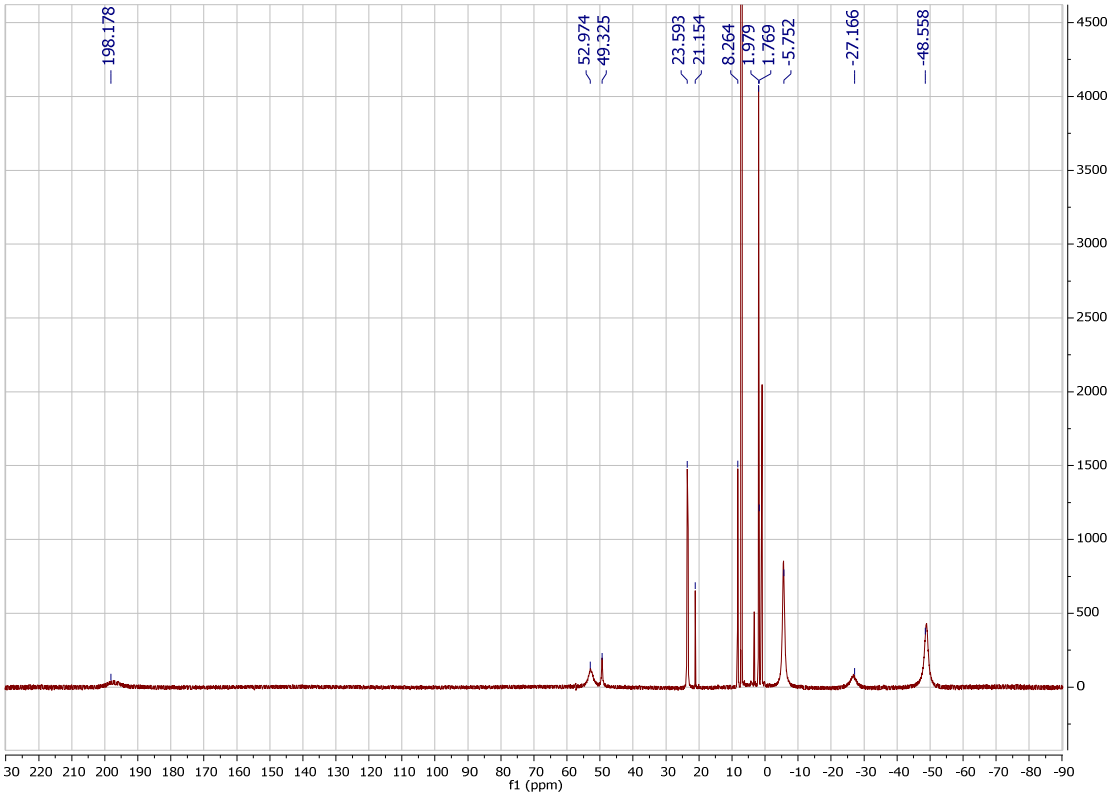

Figure S7. ^{1}H NMR of **7** in C_6D_6 (300 MHz, 298 K)

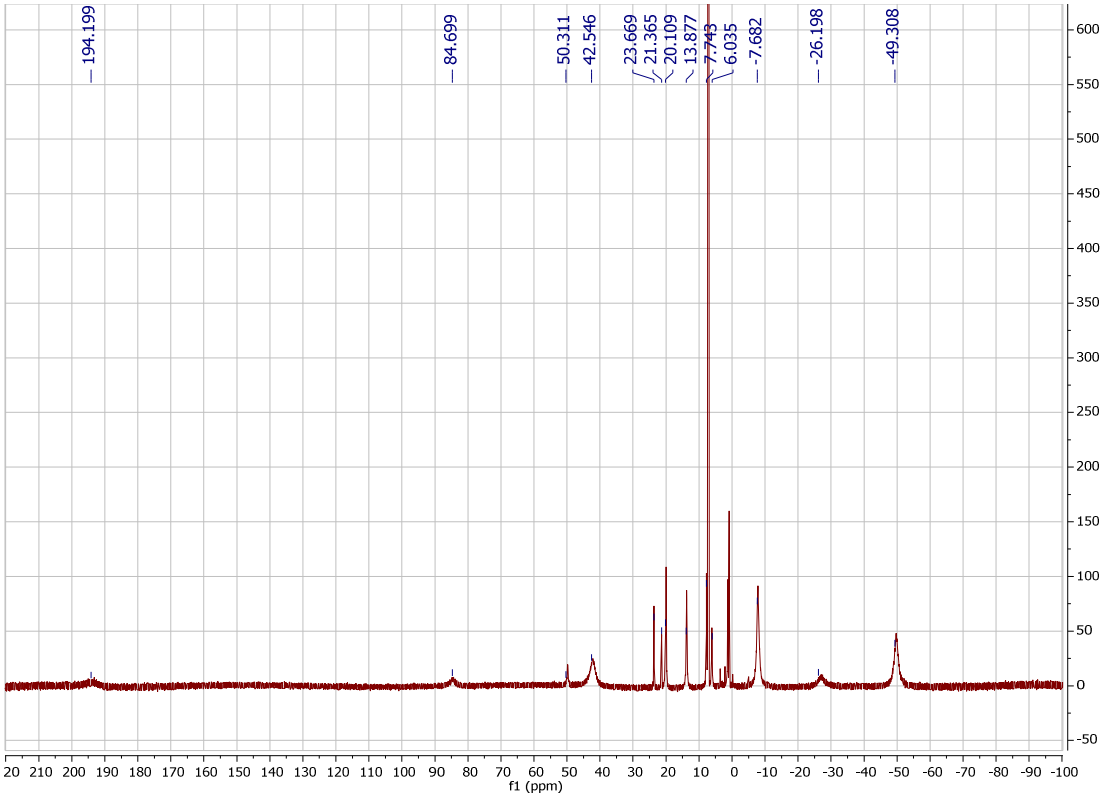

Figure S8. ^{1}H NMR of **8** in C_6D_6 (300 MHz, 298 K)

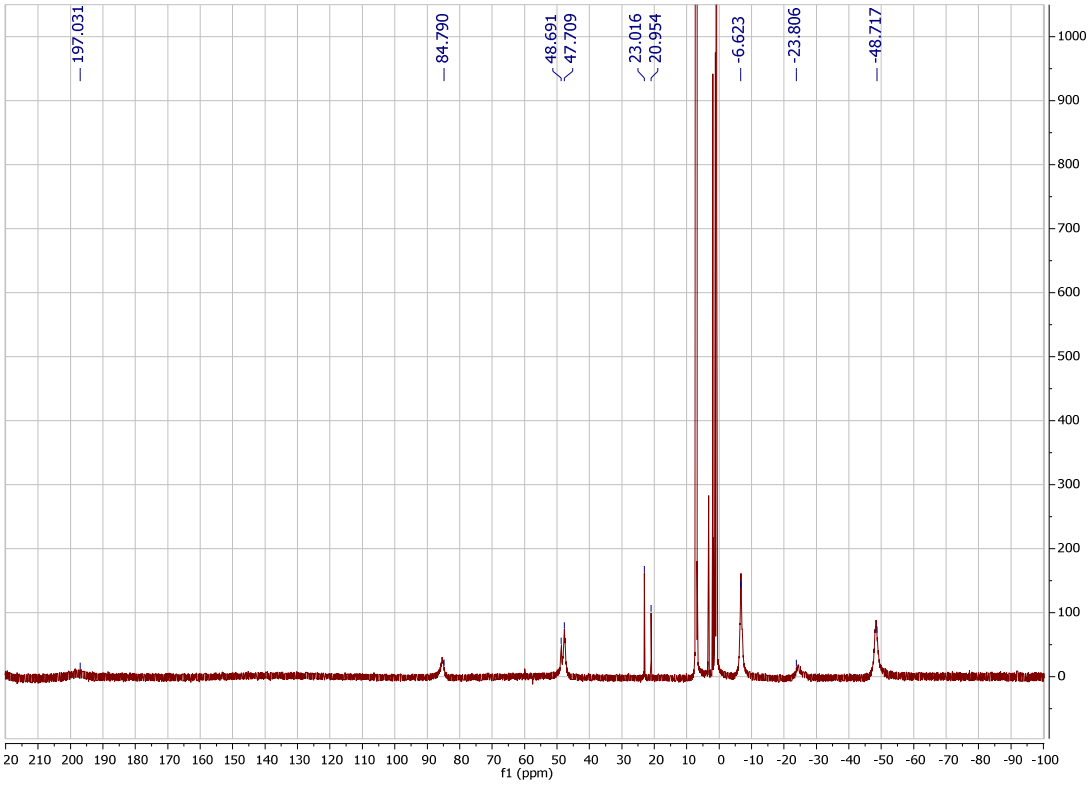

Figure S9. ^{1}H NMR of **9** in C_6D_6 (300 MHz, 298 K)

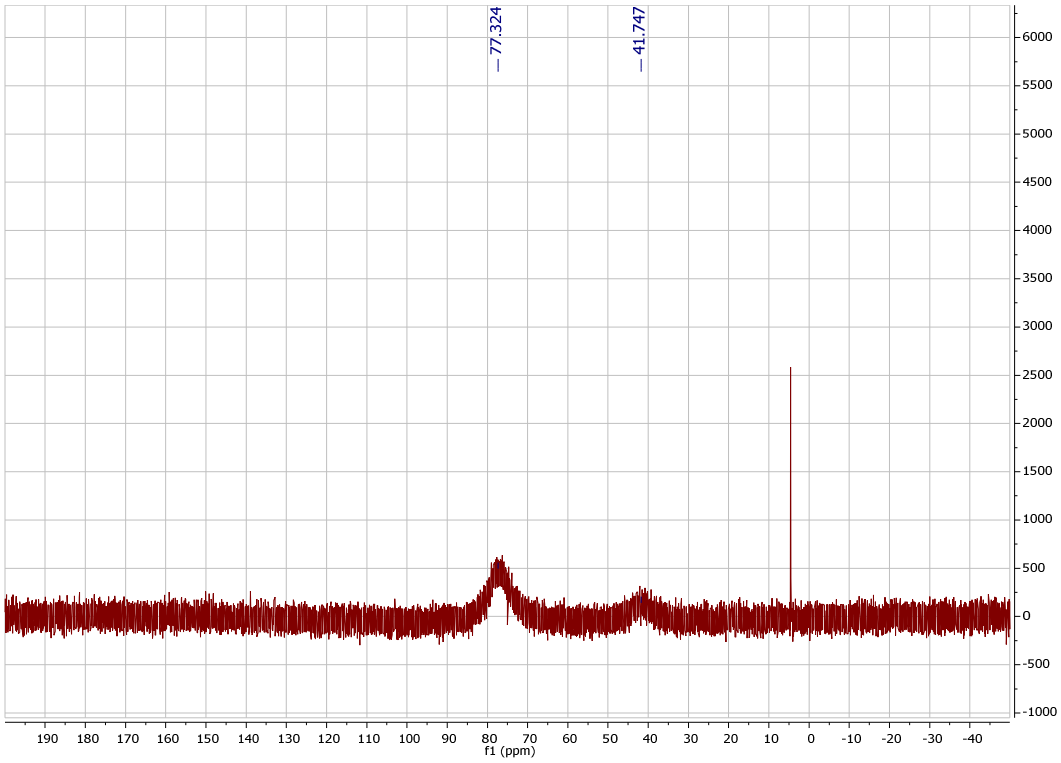

Figure S10. ^{31}P NMR of **3** in d_8-toluene (202 MHz, 198 K). The impurity is PPh_3, present in very small amounts.

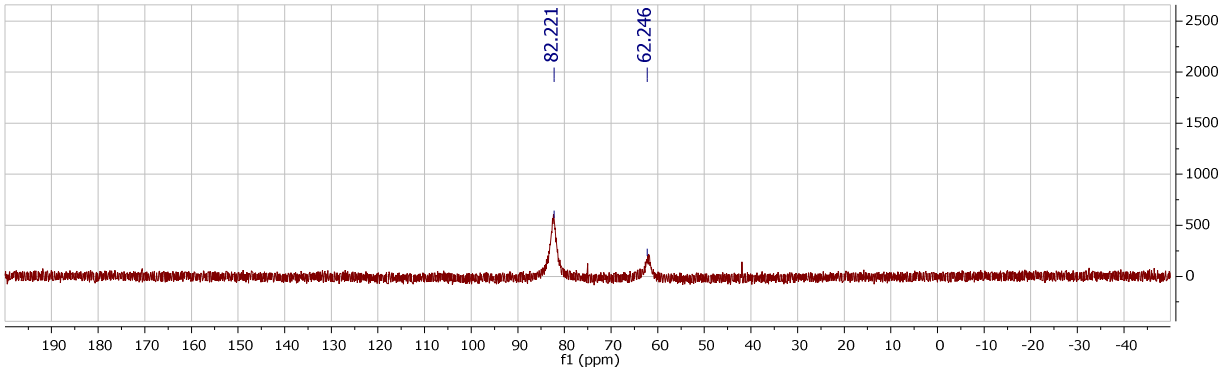

Figure S11. ^{31}P NMR of **4** in d_8-toluene (202 MHz, 198 K)

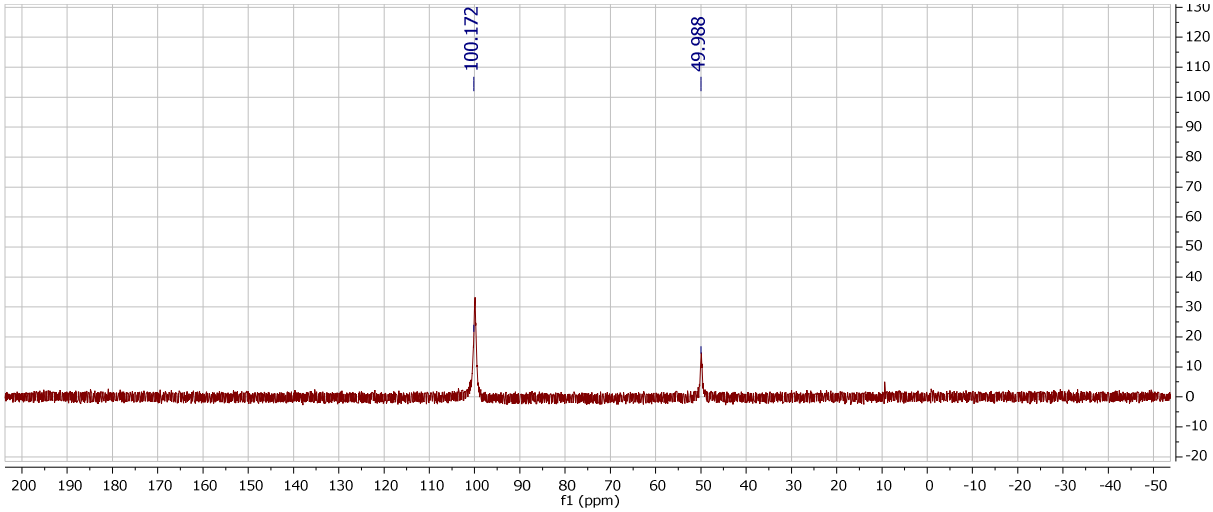

Figure S12. ^{31}P NMR of **5** in d_8-toluene (152 MHz, 198 K)

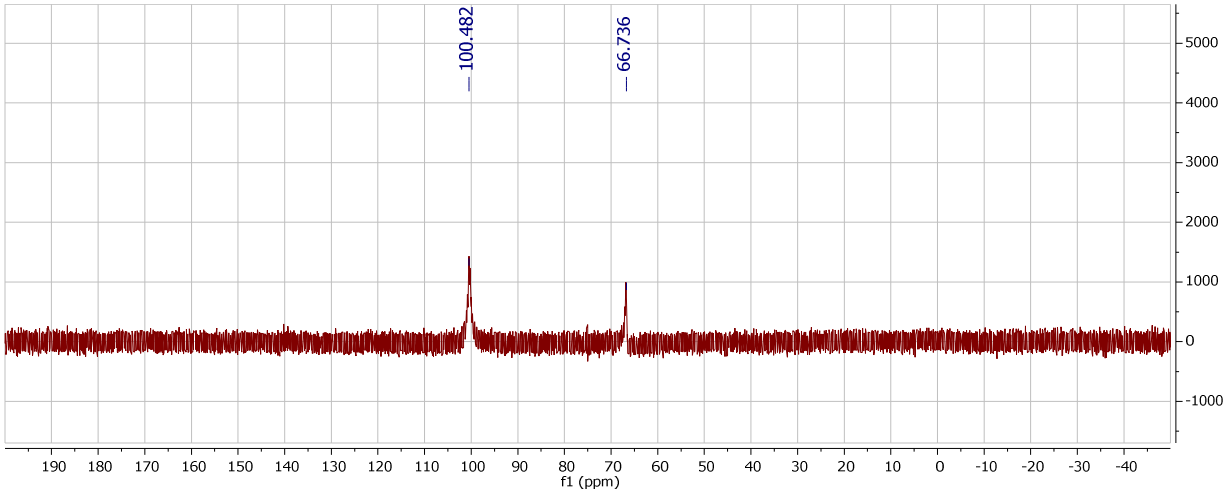

Figure S13. ^{31}P NMR of **6** in d_8-toluene (202 MHz, 188 K)

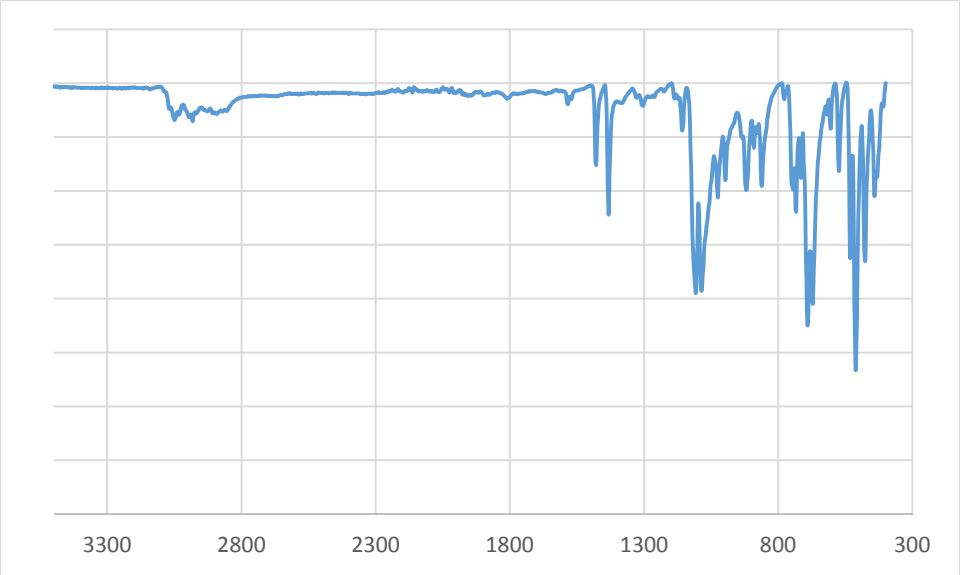

Figure S14. Infrared spectrum (298 K) of **1** as a powdered solid.

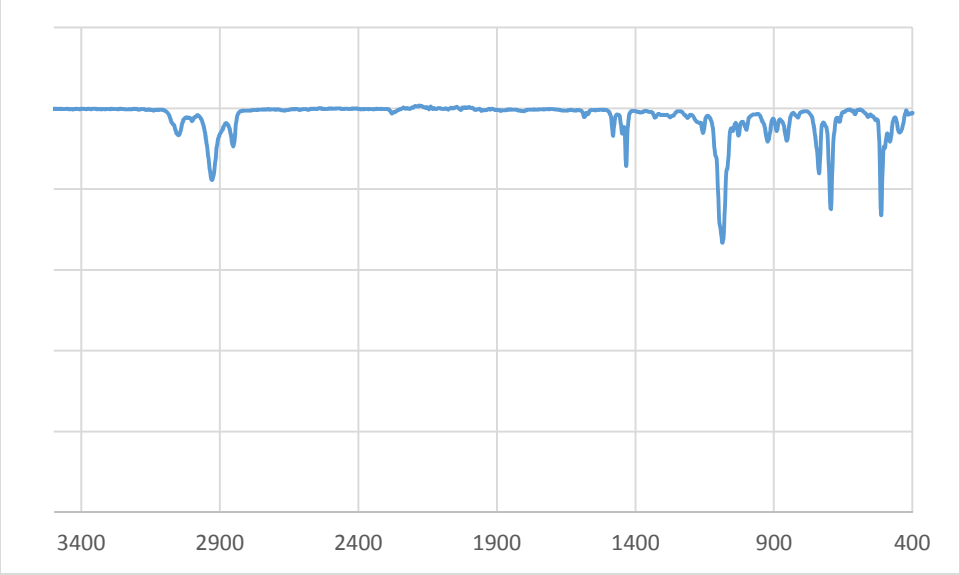

Figure S15. Infrared spectrum (298 K) of **2**, deposited as a thin film from benzene solution.

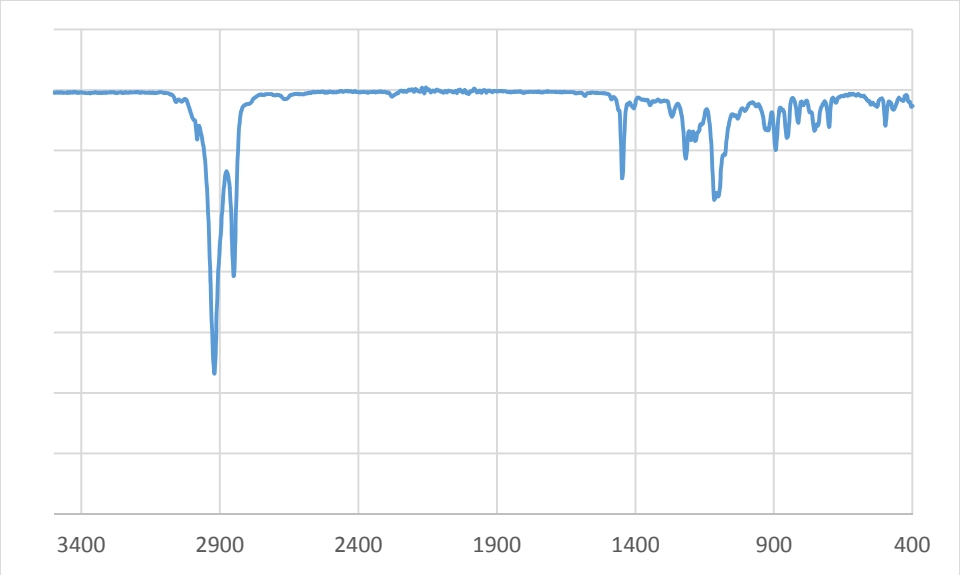

Figure S16. Infrared spectrum (298 K) of **4**, deposited as a thin film from benzene.

II. Variable-temperature NMR spectroscopy

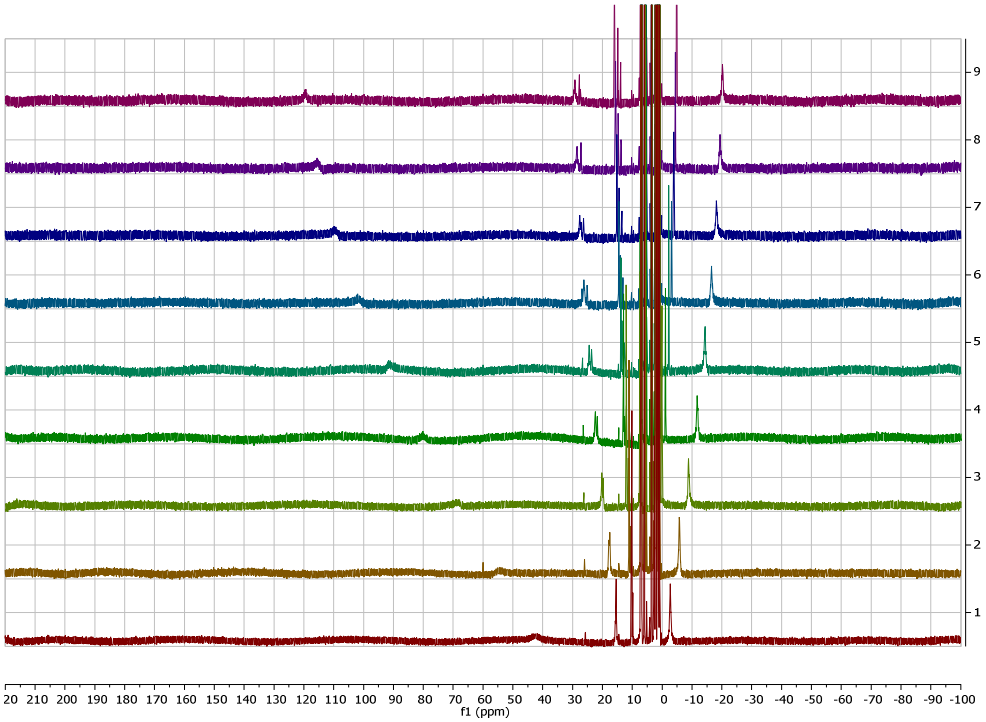

Figure S17. Variable-temperature ^{1}H NMR of **1** from 298 K (bottom) to 388 K (top) in d_8-toluene (0.015 M; 500 MHz).

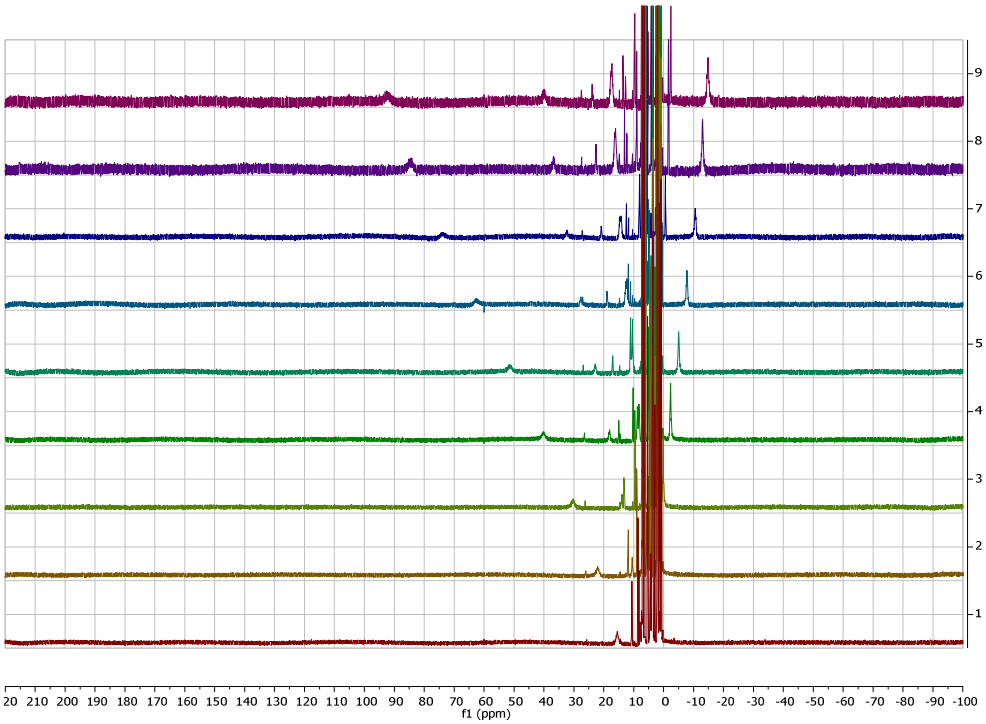

Figure S18. Variable temperature ^{1}H NMR spectra of **2** from 298 K (bottom) to 378 K (top) in d_8-toluene (0.013 M; 500 MHz).

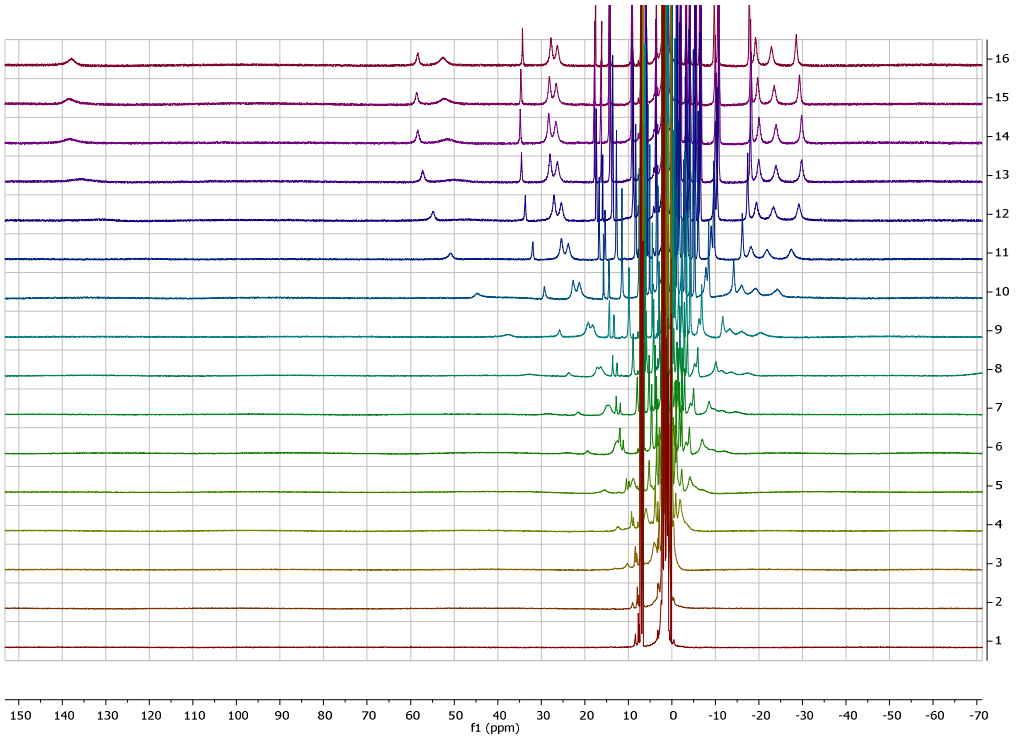

Figure S19. Variable-temperature ^{1}H NMR spectra of **4** from 223 K (bottom) to 358 K (top) in d_8-toluene (0.032 M; 500 MHz).

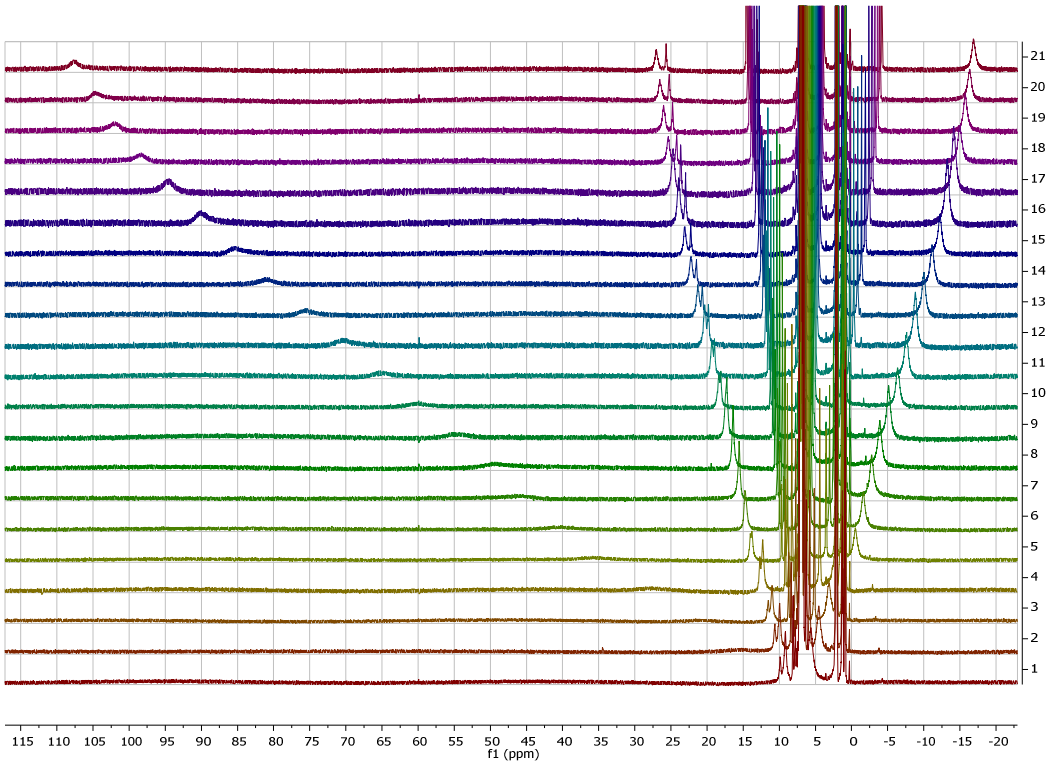

Figure S20. Variable-temperature ^{1}H NMR spectra of **5** from 258 K (bottom) to 378 K (top) in d_8-toluene (0.012 M; 500 MHz).

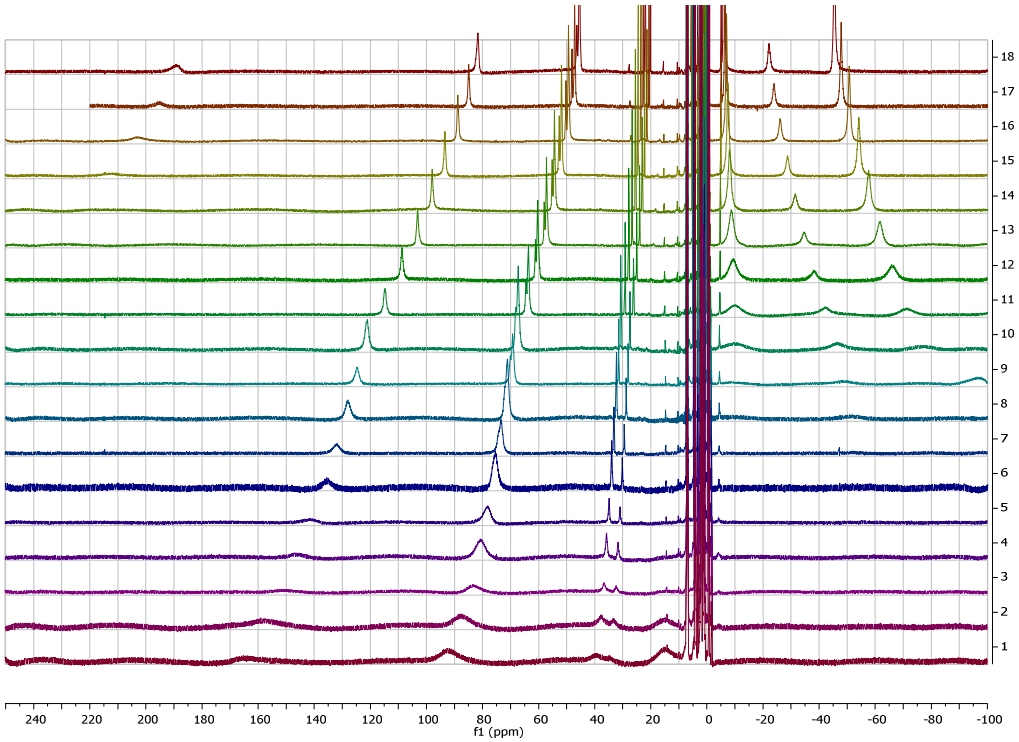

Figure S21. Variable-temperature NMR spectra of **9** from 283 K (bottom) to 408 K (top) in d_8-toluene (0.4 M; 500 MHz).

Fits to the variable-temperature NMR chemical shifts were carried out using the following model:

$$\delta = \delta_{ls} + C/(T*(1+\exp(\Delta H^{\circ}/R*(1/T-1/T_{1/2})))) \qquad \text{Equation S1}$$

where the parameters are as defined in the main text (Equation 2). Fit parameters, confidence bounds, and goodness-of-fit parameters are given below for each species.

The adjusted R^2 value is calculated as follows:

$$SSE = \sum_{i=1}^{n} \left(y_{i,obs} - y_{i,calc}\right)^2$$

$$SST = \sum_{i=1}^{n} \left(y_{i,obs} - \bar{y}\right)^2$$

$$Adj.R^2 = 1 - \frac{SSE(n-1)}{SST(n-m)}$$

Where *n* is the number of data points, $y_{i,obs}$ is the experimental value for data point *i*, $y_{i,calc}$ is the corresponding value calculated from the fit equation, $\bar{y}$ is the mean of the observed values, and *m* is the number of fit parameters.

The root-mean-square-error (RMSE) is calculated as follows:

$$RMSE = \sqrt{\frac{SSE}{(n-m)}}$$

where the parameters *SSE*, *n*, and *m* are defined as above.

The fits to the modified Curie law expression are generally good over the temperature regime where the chemical shifts are either monotonically increasing or decreasing, however the fit tends to become poor in the high-temperature regime where the high-spin state is close to fully occupied and the chemical shifts tend back towards δ_{ls}, in complexes where this regime is accessible. This may suggest that the chemical shifts of the high-spin state do not display simple Curie behavior, or that some other assumption of the model is inadequate, illustrating a possible weakness of this model. For the purposes of this study these points were excluded from the fit in order to maintain consistency between different complexes; attempting to include them (when applicable) typically results in a higher apparent value for ΔH as well as a significantly poorer overall fit (see below).

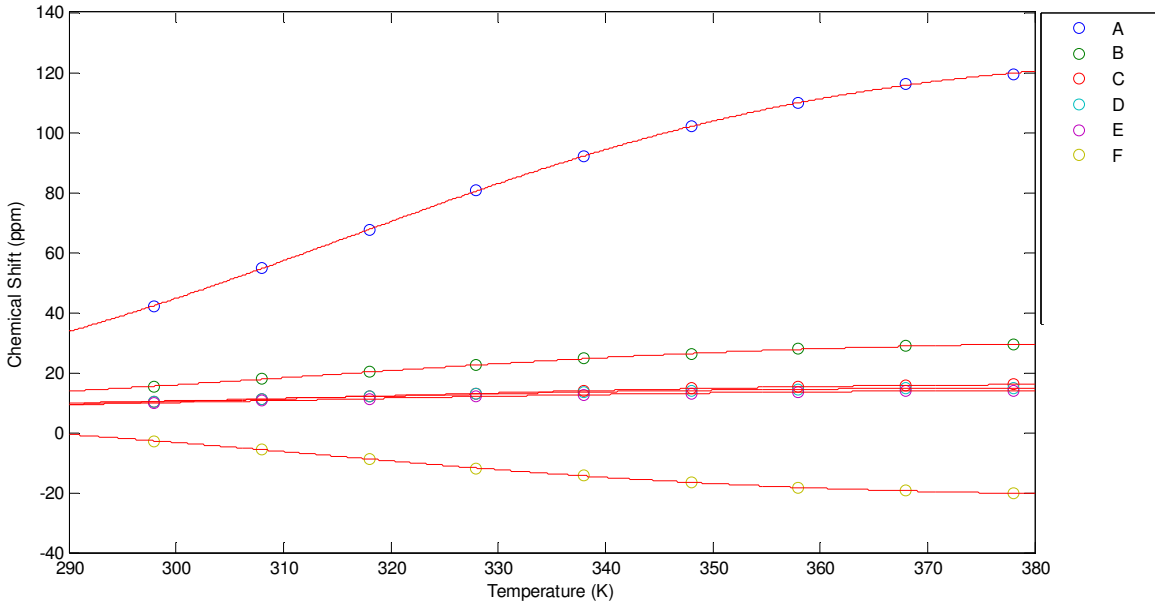

Figure S22. Variation of the chemical shifts in the ^{1}H NMR of **1** with temperature, and fits to Equation S1.

	A	**B**	**C**	**D**	**E**	**F**
δ_{ls} (ppm)	4.387 [-4.921, 13.7]	8.249 [7.167, 9.331]	7.017 [6.08, 7.954]	7.735 [7.13, 8.34]	7.836 [7.628, 8.044]	6.052 [3.78, 8.324]
C (K)	54930 [48520, 61350]	9909 [9199, 1062]	4317 [3667, 4968]	3298 [2928, 3667]	2771 [2642, 2901]	-12000 [-13420, -10580]
ΔH^o (kJ/mol)	31.4 [27.7, 35.0]	31.5 [29.3, 33.7]	30.1 [25.7, 34.5]	31.3 [27.9, 34.6]	33.6 [32.0, 35.17	33.0 [29.1, 36.9]
$T_{1/2}$ (K)	333.3 [331.9, 334.7]	331.3 [330.5, 332.1]	333.5 [331.7, 335.2]	327.9 [326.7, 329.1]	329.2 [328.6, 329.7]	329.3 [327.9, 330.6]
Adj. R^2	0.9999	1.000	0.9998	0.9999	1.000	0.9999
RMSE	0.2853	0.0313	0.0256	0.0151	0.0067	0.0697

Table S1. Fit parameters to Equation S1 for variable-temperature NMR data for compound **1**. 95% confidence bounds for each fit parameter are provided in brackets following the fitted value.

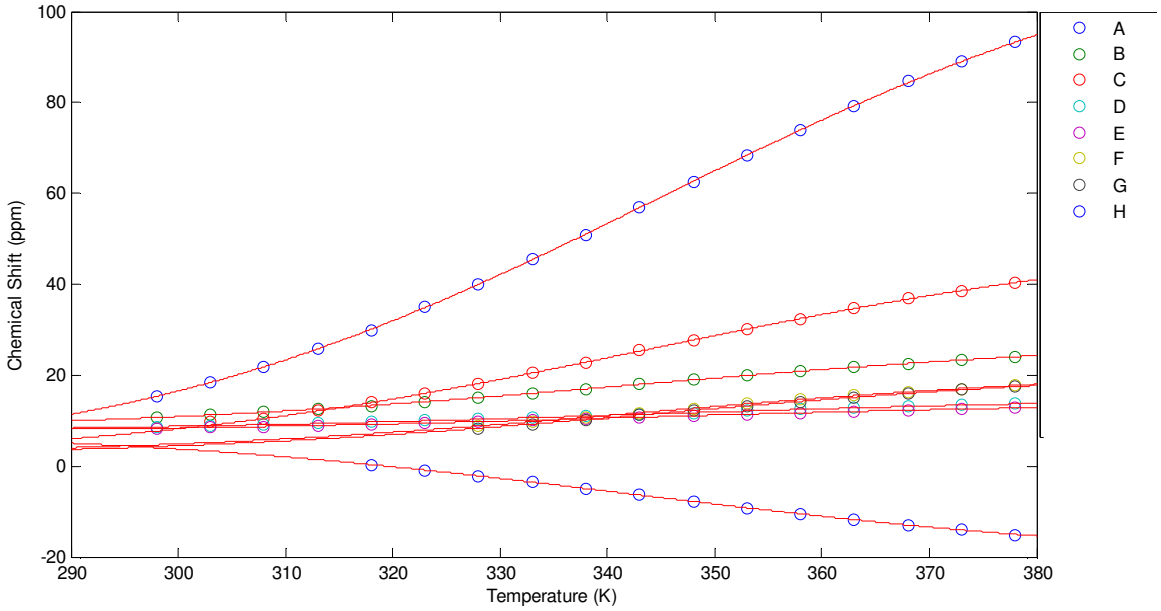

Figure S23. Variation of the chemical shifts in the ^{1}H NMR of **2** with temperature, and fits to Equation S1.

	A	**B**	**C**	**D**	**E**	**F**	**G**	**H**
δ_{ls} (ppm)	1.589 [0.1945, 2.984]	8.156 [7.783, 8.529]	1.959 [0.9927, 2.925]	7.702 [7.623, 7.78]	7.542 [7.458, 7.627]	2.595 [0.3069, 4.884]	2.409 [0.4536, 4.364]	7.359 [5.758, 8.96]
C (K)	56620 [53770, 59460]	9547 [8864, 10230	23170 [21700, 24630]	3604 [3458, 3750]	3057 [2907, 3208]	8744 [6633, 10860]	8746 [6864, 10630]	-13080 [-14870, -11280]
ΔH^{o} (kJ/mol)	34.9 [33.5, 36.4]	34.7 [32.6, 36.8]	35.4 [33.5, 37.4]	34.6 [33.4, 35.8]	36.2 [34.7, 37.8]	37.4 [29.0, 45.8]	38.4 [30.7, 46.1]	36.1 [31.5, 40.6]
$T_{1/2}$ (K)	363.2 [361, 365.4]	360.9 [357.9, 363.9]	361.5 [359.2, 363.8]	361.4 [359.7, 363.1]	359.4 [357.5, 361.4]	359 [355.2, 362.7]	359.9 [356.2, 363.6]	359.2 [355.8, 362.6]
Adj. R^2	1.000	0.9999	1.000	1.000	0.9999	0.9999	0.9999	0.9999
RMSE	0.1741	0.0439	0.0668	0.0092	0.0111	0.0368	0.0354	0.0545

Table S2. Fit parameters to Equation S1 for variable-temperature NMR data for compound **2**. 95% confidence bounds for each fit parameter are provided in brackets following the fitted value.

For complex **3**, as discussed above, the fit to Equation S1 for points above about 300 K is very poor, and thus these were omitted from the fit for the purposes of calculating ΔH^o and $T_{1/2}$; the effect of including these points will be shown below.

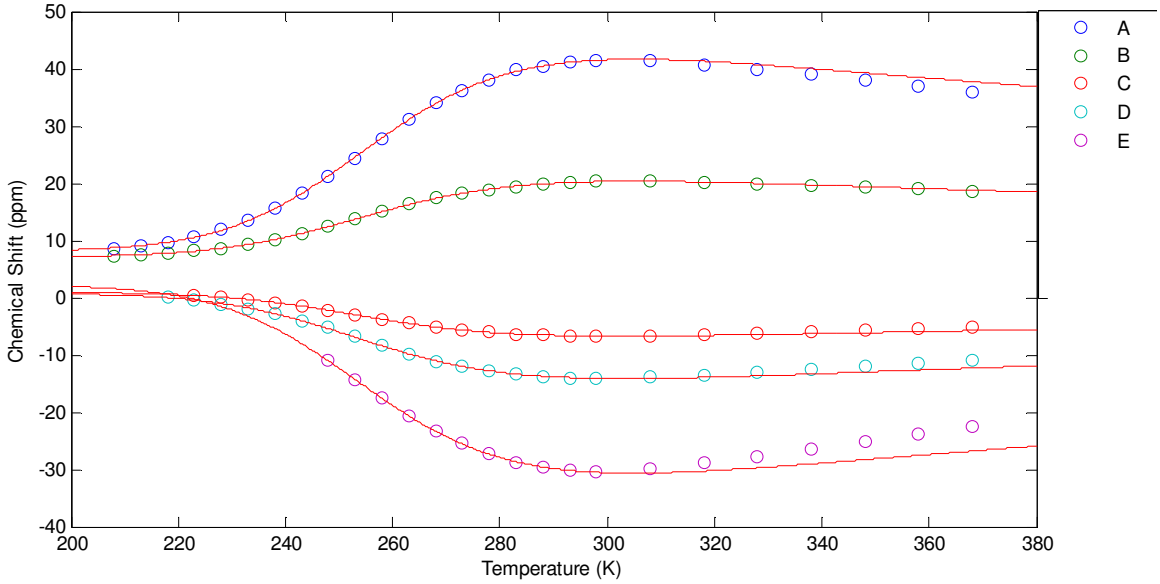

Figure S24. Variation of the chemical shifts in the ^{1}H NMR of **3** with temperature, and fits to Equation S1 with points above 300 K omitted from the fits.

	A	**B**	**C**	**D**	**E**
δ_{ls} (ppm)	8.144 [7.876, 8.351]	7.121 [7.021, 7.221]	0.9464 [0.8106, 1.082]	0.7459 [0.4437, 1.048]	2.253 [-4.666, 9.172]
C (K)	10970 [10770, 11160]	4326 [3065, 3247]	-2477 [-2553, -2402]	-4825 [-5014, -4637]	-10750 [-13440, -8055]
ΔH^o (kJ/mol)	38.3 [37.2, 39.4]	37.8 [36.7, 38.8]	39.4 [37.6, 41.2]	38.5 [36.2, 40.8]	37.9 [29.2, 46.7]
$T_{1/2}$ (K)	260 [259.5, 260.4]	259.7 [259.2, 260.1]	258.6 [258.1, 259.1]	258.6 [257.9, 259.4]	259.5 [256.6, 262.3]
Adj. R^2	0.9999	0.9999	0.9998	0.9995	0.9995
RMSE	0.1449	0.0590	0.0393	0.1127	0.1504

Table S3. Fit parameters to Equation S1 for variable-temperature NMR data for compound **3,** with points above 300 K omitted from the fits. 95% confidence bounds for each fit parameter are provided in brackets following the fitted value.

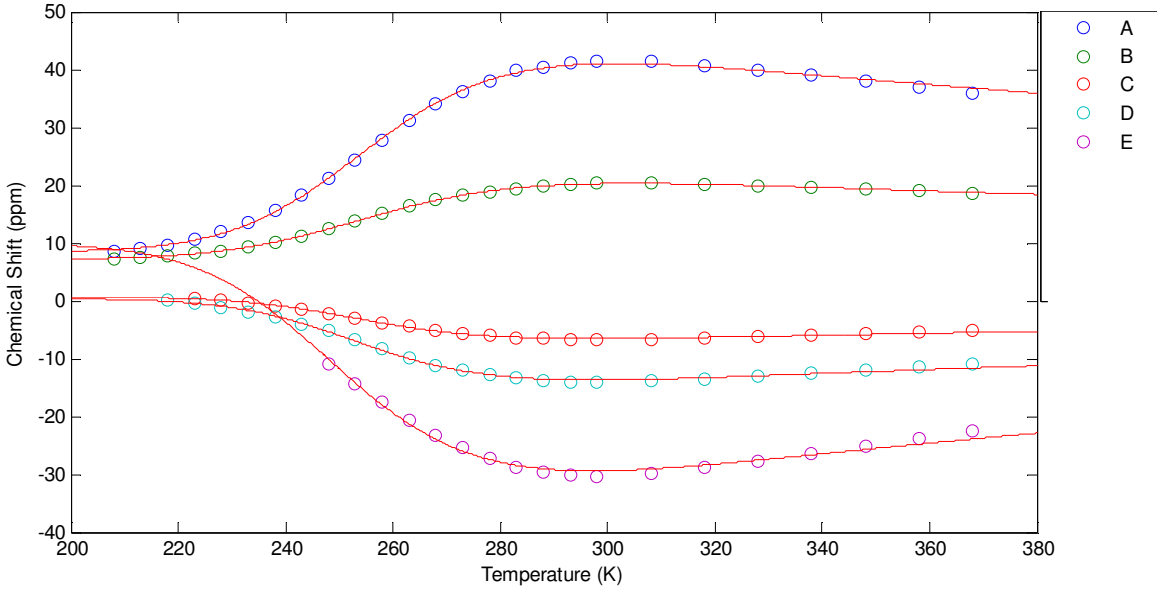

Figure S25. Variation of the chemical shifts in the ^{1}H NMR of **3** with temperature, and fits to Equation S1 with all points included in the fits.

	A	**B**	**C**	**D**	**E**
δ_{ls} (ppm)	8.416 [7.948, 8.884]	7.141 [7.053, 7.229]	0.7681 [0.425, 1.111]	0.4002 [-0.1672, 0.9676]	10[a]
C (K)	10480 [10270, 10700]	4297 [4256, 4338]	-2299 [-2436, -2163]	-4434 [-4668, -4200]	-12520 [-12760, -12280]
ΔH^o (kJ/mol)	41.0 [39.2, 42.8]	38.2 [37.5, 38.9	44.2 [39.7, 48.8]	43.8 [39.5, 48.2]	38.2 [34.4, 42.0]
$T_{1/2}$ (K)	258.8 [258.3, 259.4]	259.5 [259.2, 259.7]	257.3 [256.2, 258.4]	257 [255.9, 258.1]	253.7 [252.6, 254.7]
Adj. R^2	0.9992	0.9999	0.9969	0.9967	0.9829
RMSE	0.3413	0.598	0.1358	0.2859	0.7361

Table S4. Fit parameters to Equation S1 for variable-temperature NMR data for compound **3,** with all points included in the fits. 95% confidence bounds for each fit parameter are provided in brackets following the fitted value. [a]Fit value fixed at upper limit.

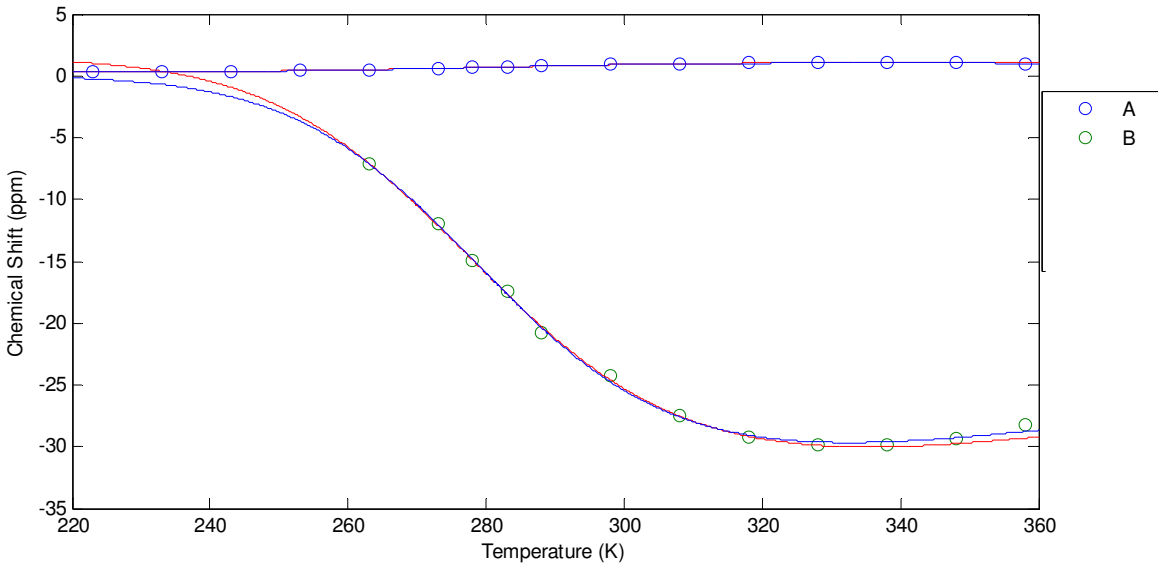

Figure S26. Variation of the chemical shifts in the ^{1}H NMR of **4** with temperature, and fits to Equation S1 with points above 300 K omitted (red lines) or included (blue lines).

	A, <300 K	**B, <300 K**	**A, all**	**B, all**
δ_{ls} (ppm)	0.321 (0.3126, 0.3294)	1.468 [-4.324, 7.26]	0.3286 [0.316, 0.3413]	0.01366 [-4.133, 4.16]
C (K)	272.5 [260.5, 284.4]	-11340 [-14060, -8624]	253.9 [246.1, 261.7]	-10520 [-12220, -8828]
ΔH^o (kJ/mol)	39.3 [37.12, 41.5]	40.2 [29.4, 51.0]	42.9 [40.2, 45.7]	44.2 [36.0, 52.3]
$T_{1/2}$ (K)	288.1 [286.7, 289.5]	284.5 [281.8, 287.2]	286 [285, 286.9]	284.5 [282, 287]
Adj. R^2	0.9997	0.9986	0.9992	0.9980
RMSE	0.0040	0.3033	0.0078	0.3557

Table S5. Fit parameters to Equation S1 for variable-temperature NMR data for compound **4.** 95% confidence bounds for each fit parameter are provided in brackets following the fitted value.

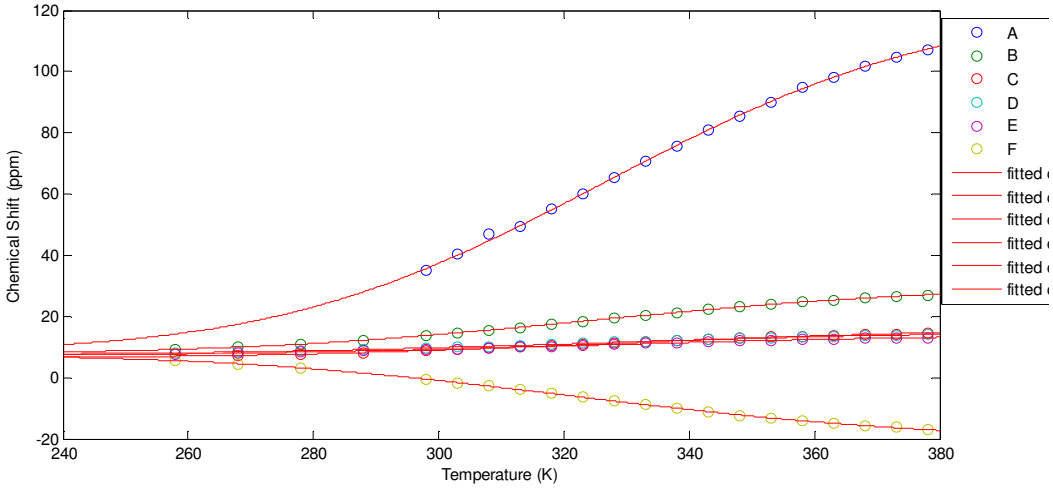

Figure S27. Variation of the chemical shifts in the ^{1}H NMR of **5** with temperature, and fits to Equation S1.

	A	**B**	**C**	**D**	**E**	**F**
δ_{ls} (ppm)	8.767 [3.712, 13.82]	7.798 [7.571, 8.026]	6.457 [6.348, 6.566]	7.574 [7.479, 7.668]	7367 [7.318, 7.415]	7.651 [7.409, 7.892]
C (K)	53920 [48630, 59220]	10890 [10430, 11350]	4664 [4461, 4867]	3673 [3486, 3860]	3219 [3124, 3315]	-13860 [-14340, 13390]
ΔH^{o} (kJ/mol)	29.7 [26.9, 32.4]	27.2 [26.2, 28.2]	27.5 [26.5, 28.5]	26.6 [25.4, 27.7]	27.2 [26.5, 27.9]	26.3 [25.5, 27.1]
$T_{1/2}$ (K)	348.5 [345.7, 351.3]	349.6 [347.2, 352]	351.9 [349.6, 354.3]	349.3 [346.4, 352.3]	348.7 [347, 350.4]	348.5 [346.5, 350.4]
Adj. R^2	0.9999	0.9999	0.9999	0.9998	0.9999	0.9999
RMSE	0.2827	0.0609	0.0214	0.0237	0.0129	0.0579

Table S6. Fit parameters to Equation S1 for variable-temperature NMR data for compound **5.** 95% confidence bounds for each fit parameter are provided in brackets following the fitted value.

Variable temperature Evans method data (corrected for density changes) was fit to the following equation:

$$\chi T = (\chi T)_{HS}/(1+\exp(\Delta H^{o}/R*(1/T-1/T_{1/2})))+ (\chi T)_{LS} \qquad \text{Equation S2}$$

Although the resulting fits are not unreasonable, except for complex **3** (for which the largest range of the transition was probed) the uncertainties (as represented by the 95% confidence bounds) in the fit parameters are very large. The temperature over which χT could be measured is limited for most complexes both by the boiling/freezing points of the solvents as well as the fact that at temperatures well below $T_{1/2}$ the very small magnetic moment is difficult to determine accurately from the Evans method shift.

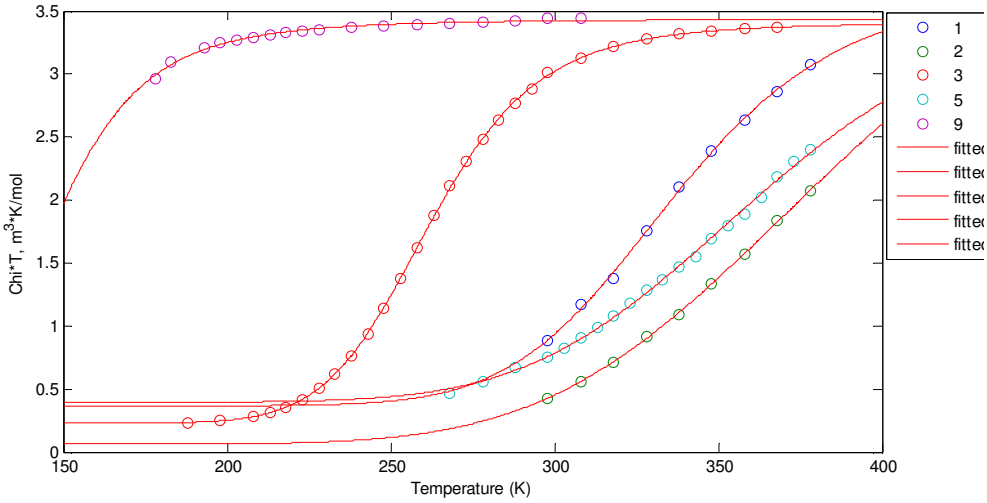

Figure S28. Variable temperature Evans method data, with fits to Equation S2.

	1	**2**	**3**	**5**	**9**
$(\chi T)_{HS}$ (m^3K/mol)	3.365 [2.267, 4.464]	4.777 [1.223, 8.331]	3.181 [3.164, 3.197]	3.5 [2.522, 4.478]	3.379 [-16.28, 23.03]
ΔH^o (kJ/mol)	35.8 [20.9, 50.7]	25.2 [14.2, 36.2]	33.9 [33.5, 34.4]	28.1 [22.5, 33.8]	12.7 [5.0, 20.4]
$T_{1/2}$ (K)	337.2 [331.1, 343.3]	393.4 [332.7, 454]	262.1 [261.8, 262.3]	367.4 [348.5, 386.3]	146.3 [39.15, 253.4]
$(\chi T)_{LS}$ (m^3K/mol)	0.3665 [-0.1379, 0.8709]	0.06145 [-0.2008, 0.3237]	0.2266 [0.2168, 0.2363]	0.3954 [0.3053, 0.4856]	0.05959 [-19.57, 19.69]
Adj. R^2	0.9983	0.9994	0.9999	0.9981	0.9880
RMSE	0.320	0.0136	0.0093	0.0256	0.0137

Table S7. Fit parameters to Equation S2 for variable-temperature Evans method data for compounds **1-3**, **5**, and **9.** 95% confidence bounds for each fit parameter are provided in brackets following the fitted value. Nonzero values for $(\chi T)_{LS}$ may reflect either paramagnetic impurities or uncertainties in the fit.

III. Variable-temperature UV-Vis spectroscopy

Several corrections must be applied to the UV-Vis data before it can be quantitatively modeled. First, due to the change in density of the solvent (toluene) with temperature, the effective concentration of the sample changes as the temperature is raised or lowered; the absorption must be multiplied by a simple scaling factor at each temperature to account for this change.[1] Secondly, due to the change in absorption lineshapes with temperature, simply charting the absorbance at λ_{max} for a given peak is inadequate.[2] Instead, the spectra at each temperature are modeled as the sum of three Gaussian functions (Equation S3, Figure S29),

$$\mathrm{Abs}(\lambda) = \sum_{n=1}^{3} \frac{c_n a_n}{\sqrt{\pi}} \exp\left(-a_n^2\left(\lambda - \lambda_{max,n}\right)\right) \qquad \text{(Equation S3)}$$

where the parameter c_n is the area of each peak, a_n is related to the width (FWHM) of the peak, and $\lambda_{max,n}$ is the wavelength of maximum absorption for each peak; more details on these fits are provided below. The areas of these Gaussian peaks (parameter c_n) are then correlated with the concentration of the low-spin species. These can be fit to a Boltzmann equilibrium expression for the spin crossover to extract thermodynamic parameters,

$$x_{ls}(\mathrm{T}) = \frac{1}{1+\exp\left(-\frac{\Delta \mathrm{H}^o}{\mathrm{R}}\left(\frac{1}{\mathrm{T}} - \frac{1}{\mathrm{T}_{1/2}}\right)\right)} \qquad \text{(Equation S4)}$$

$$x_{ls} = c/c_{max} \qquad \text{(Equation S5)}$$

where $x_{ls}(\mathrm{T})$ is the low-spin mole fraction as a function of the temperature T, c is the Gaussian fit parameter as in Equation S3, c_{max} is the value of c when $x_{ls} = 1$, *i.e.* in the low-temperature limit, ΔH^o is the enthalpy difference between the low- and high-spin states, and $T_{1/2}$ is the critical temperature, *i.e.* the temperature at which equal amounts of the high- and low-spin form are present. The enthalpy and entropy differences between the states, ΔH^o and ΔS^o ($\Delta S^o = \Delta H^o/T_{1/2}$) are assumed to be approximately independent of temperature over the range studied. A first-order baseline was included in the fits to roughly account for the tailing of absorption bands outside the modeled range; in most cases this correction is negligible. Figure S29 provides an example of the Gaussian decomposition and fits for complex **5**, while the spectral decomposition is shown for the remaining complexes in figures S30-S35.

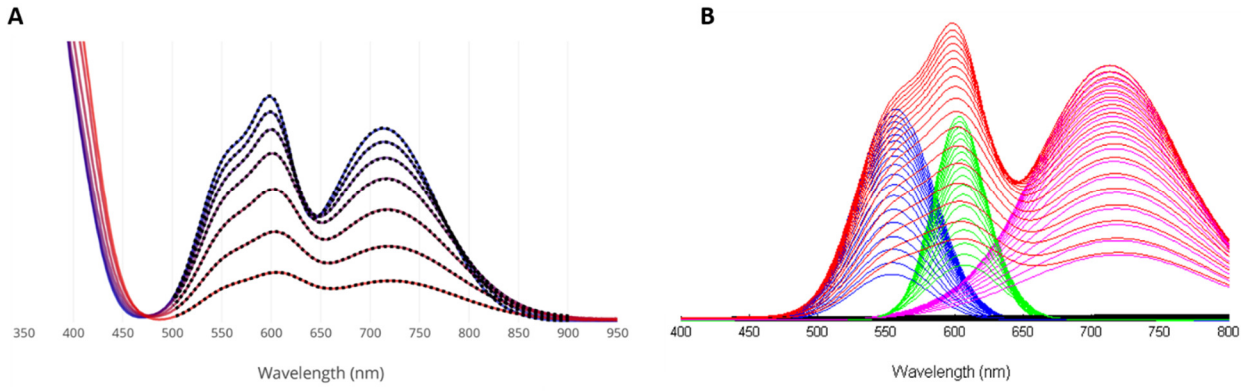

Figure S29. Example of the decomposition of the temperature-dependent UV-Vis spectra of **5** into sets of three Gaussian functions (0.20 mM in toluene). (**A**) Fits (dotted lines) to the absorbance spectra at temperatures ranging from 188 K to 383 K. For clarity, only a subset of the full data set is shown. (**B**)

Decomposition of the fitted spectra (red) into three Gaussian functions (blue, green, pink) with a minor linear baseline (black).

The temperature dependent UV-Vis spectra for complexes **1-4** are shown in Figure 4 in the main text and the resulting fits to the transition intensities according to Equations S4 and S5 for complexes **1-6** are given in Figure 6 in the main text. The maximum and minimum intensities are allowed to refine freely and only one peak (that at ~700 nm for each species) is considered. Repeating the analysis with the other major peaks, or with the total area of all three peaks, gives similar results. Robust values for the critical temperature $T_{1/2}$ are obtained in each case, while the exact values of ΔH^o and ΔS^o are subject to a higher degree of error and can fluctuate depending on the details of the fitting procedure. However, trends between different complexes are well-reproduced as long as the data are treated in a consistent fashion.

Note: in all spectral decomposition figures shown below, the red trace represents the overall (fit) spectrum, and the blue, green, and purple traces represent the individual Gaussian functions.

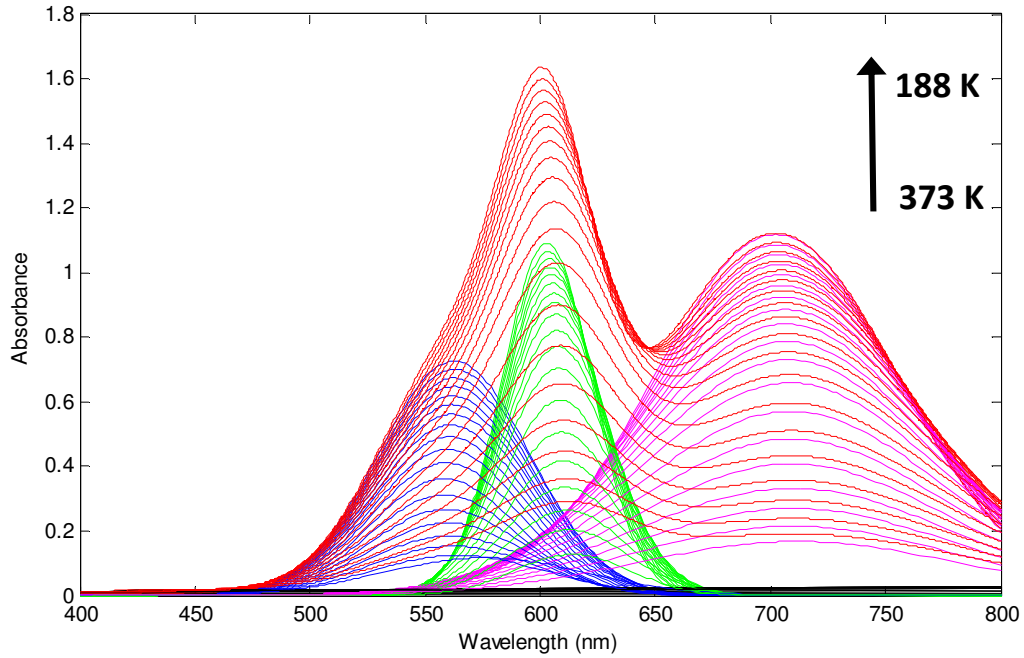

Figure S30. Spectral decomposition of the variable temperature UV-Vis spectra of **1**, (0.61 mM in toluene).

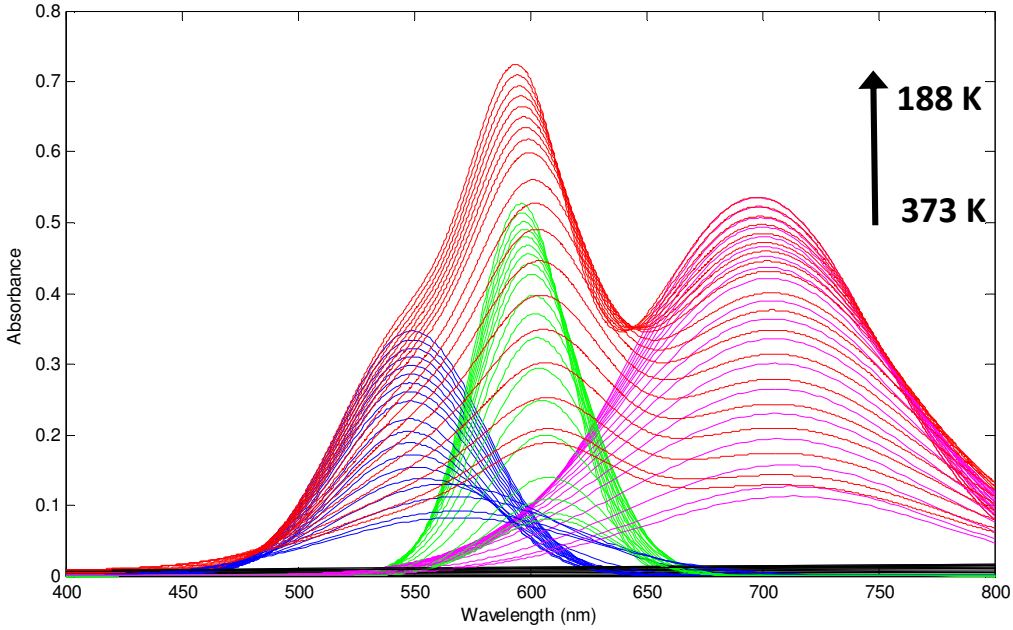

Figure S31. Spectral decomposition of the variable temperature UV-Vis spectra of **2** (0.38 mM in toluene).

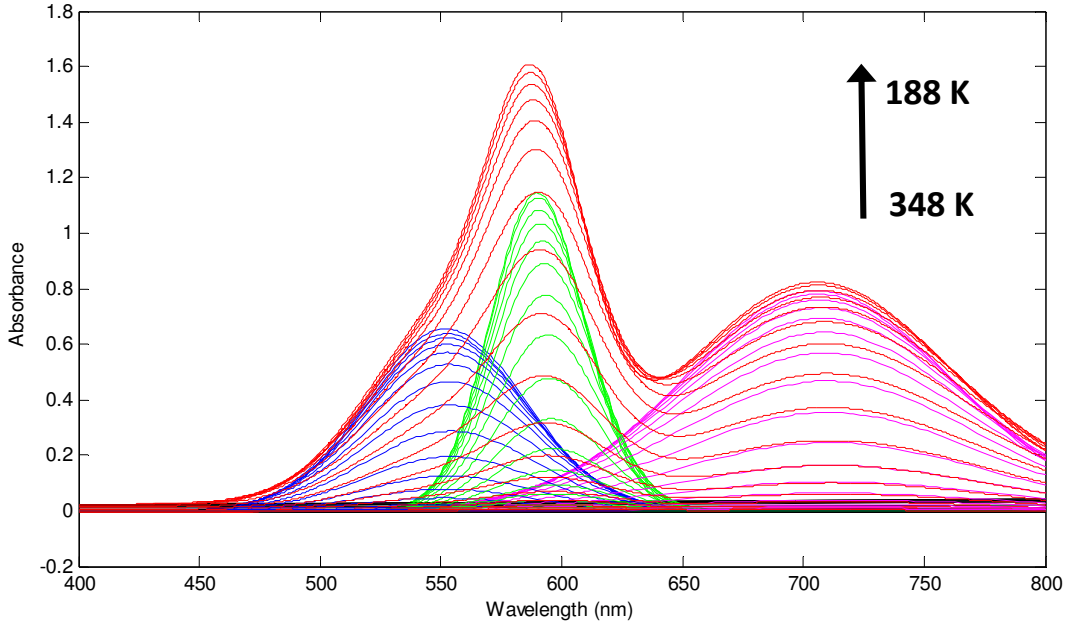

Figure S32. Spectral decomposition of the variable temperature UV-Vis spectra of **3** (0.73 mM in toluene).

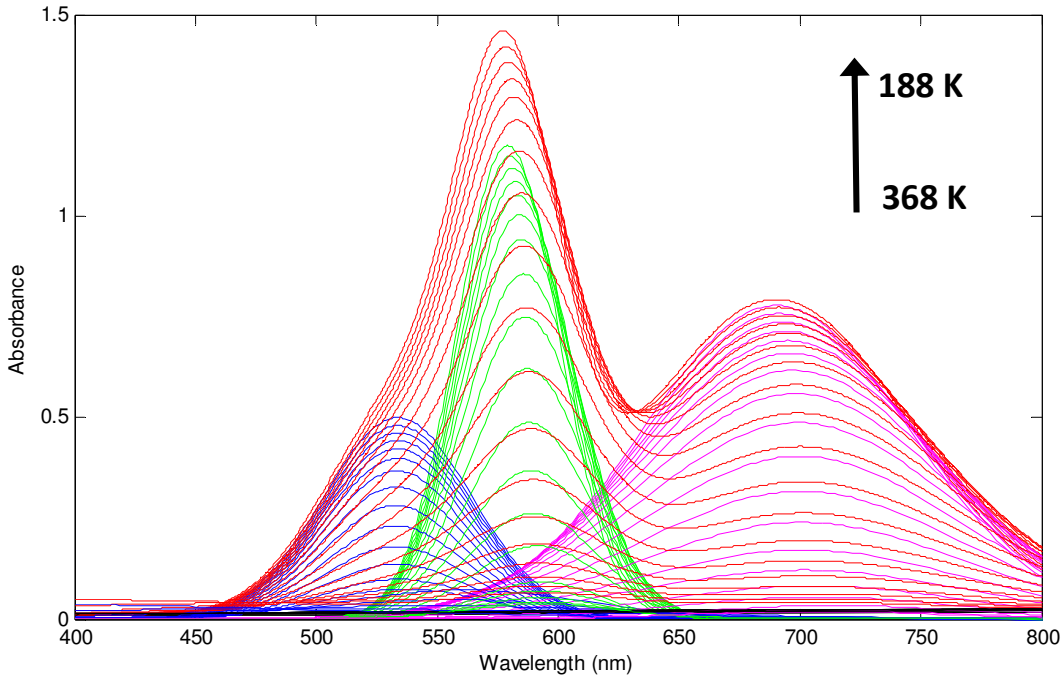

Figure S33. Spectral decomposition of the variable temperature UV-Vis spectra of **4** (1.3 mM in toluene).

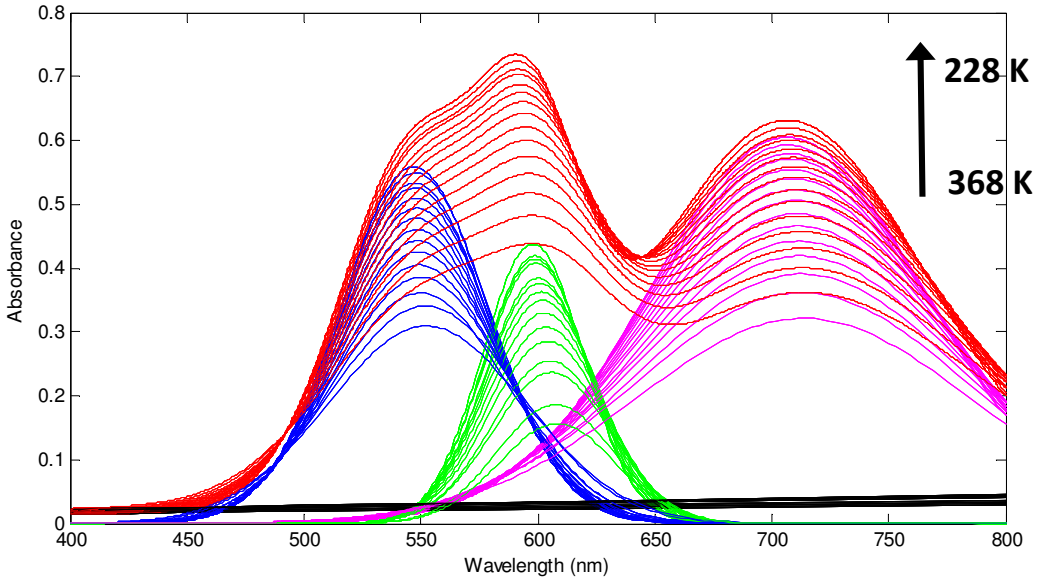

Figure S34. Spectral decomposition of the variable temperature UV-Vis spectra of **6** (0.65 mM in toluene)**.**

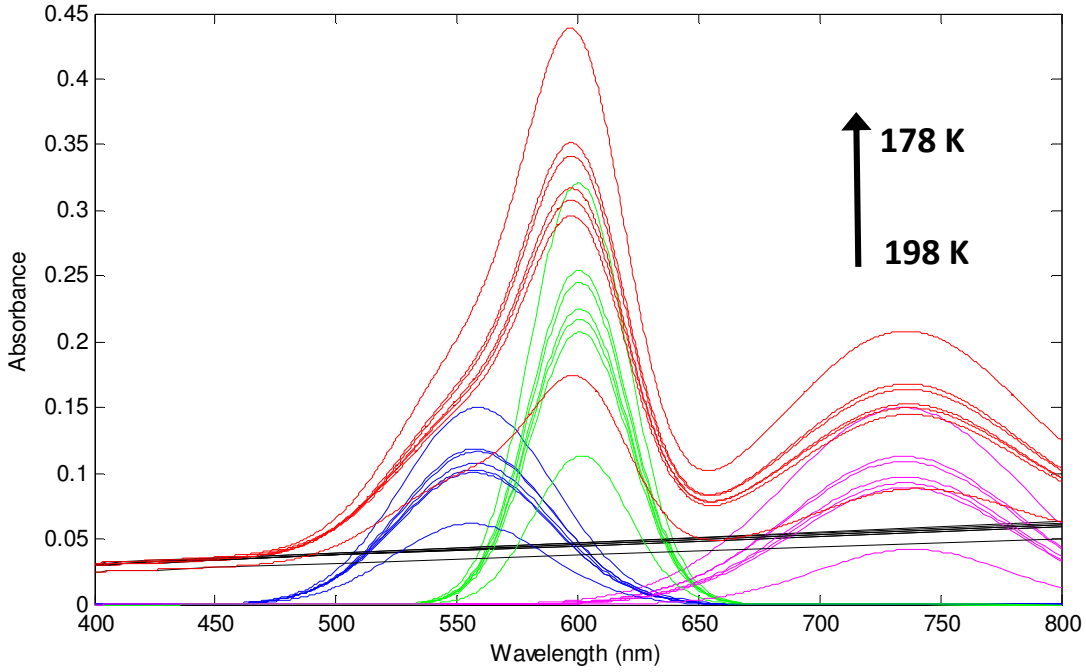

Figure S35. Spectral decomposition of the variable temperature UV-Vis spectra of **9** (2.8 mM in toluene).

	1	**2**	**3**	**4**	**5**	**6**
c_{max}	132.4 [132, 132.8]	62.85 [62.66, 63.03]	96.9 [96.57, 97.23]	96.4 [95.63, 97.17]	66.13 [65.79, 66.48]	82.99 [82.6, 83.39]
ΔH^o (kJ/mol)	32.9 [32.4, 33.4]	39.5 [38.7, 40.3]	36.3 [35.8, 36.8]	38.4 [37.1, 39.8]	30.3 [29.4, 31.2]	38.3 [34.5, 42.0]
$T_{1/2}$ (K)	332.8 [332.5, 333.2]	353.1 [352.7, 353.5]	261.2 [261, 261.5]	290.9 [290.1, 291.7]	343.2 [342.4, 344]	405.4 [400.2, 410.6]
Adj. R^2	0.9998	0.9997	0.9999	0.9995	0.9993	0.9939
RMSE	0.4909	0.2578	0.3240	0.8639	0.4341	0.4793

Table S8. Fit parameters to Equation 2 (main text) for variable-temperature UV-Vis data for compounds **1-6** (see Figure 6, Table 3, and related discussion in the main text)**.** 95% confidence bounds for each fit parameter are provided in brackets following the fitted value. RMSE and Adj. R^2 are as defined above.

Each set of variable temperature UV-Vis spectra was fit to the sum of three Gaussian functions plus a first-order baseline (Equation S6) in the relevant spectral region. Complex **1** is discussed below in detail as an example (Figure S30). Data was fit from 501 nm to 851 nm to the following equation using a least-squares fitting procedure in Matlab:

$$Abs = a * l/\sqrt{\pi} * e^{(-a^2*(x-b)^2)} + c * m/\sqrt{\pi} * e^{(-c^2*(x-d)^2)} + f * n/\sqrt{\pi} * e^{(-f^2*(x-g)^2)} + (q * x)$$

Equation S6

Parameters a, c, and f relate to the FWHM of each Gaussian function, l, m, and n are the area under the peak, and b, d, and g correspond to the wavelength of the peak maximum. The q parameter corresponds to the linear baseline term. Figures S36-S39 show the resulting fit parameters for complex **1**.

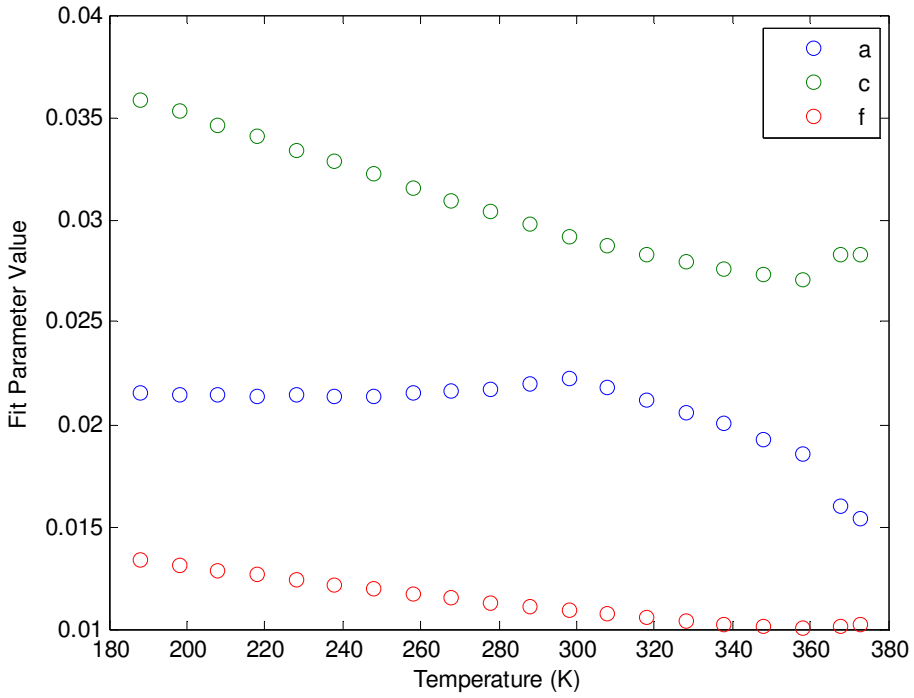

Figure S36. Fit values of the parameters a, c, and f (Equation S6) for compound **1**.

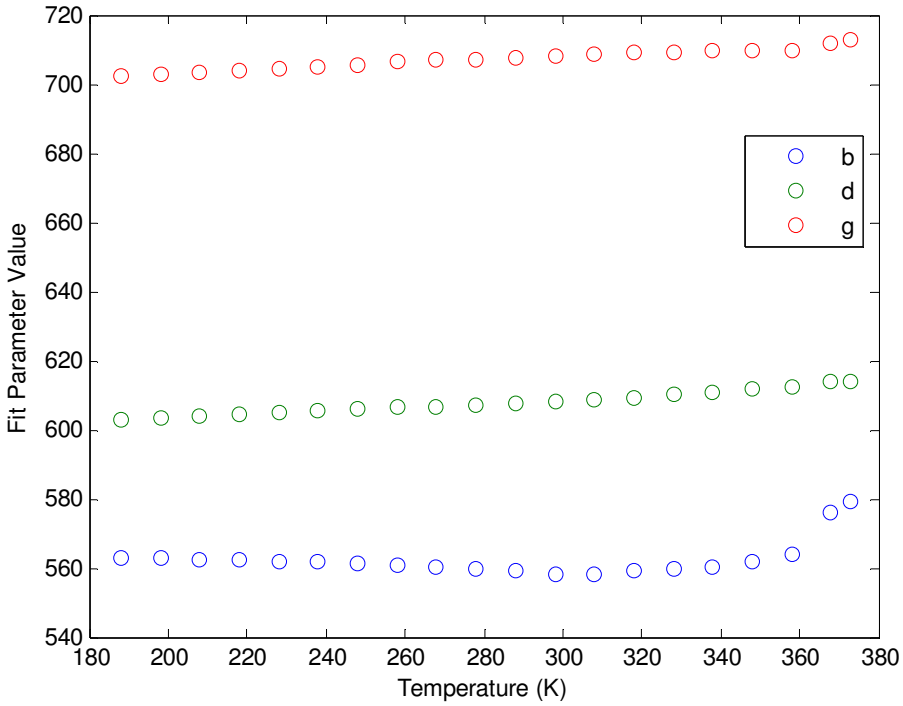

Figure S37. Fit values of the parameters b, d, and g (Equation S6) for compound **1**.

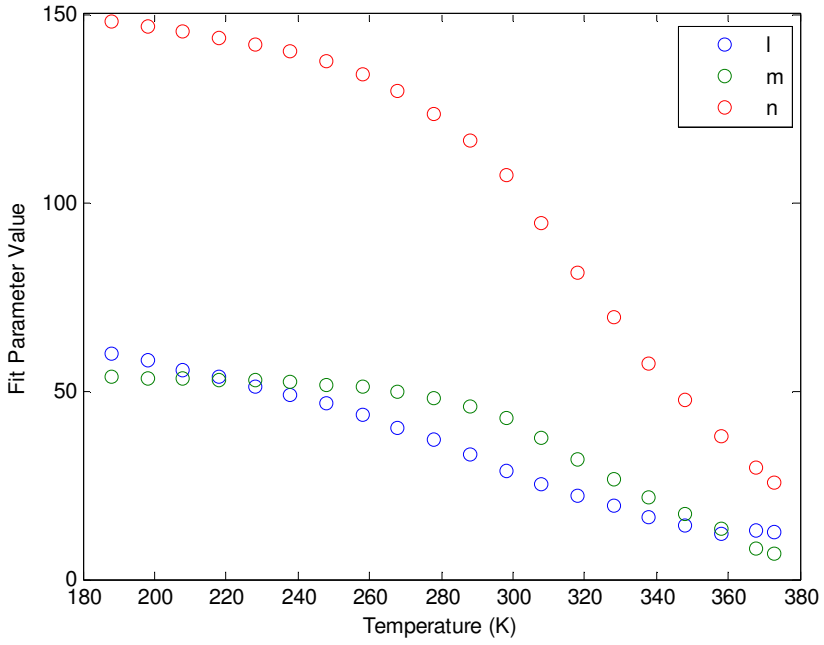

Figure S38. Fit values for the parameters l, m, and n (Equation S6) for compound **1**.

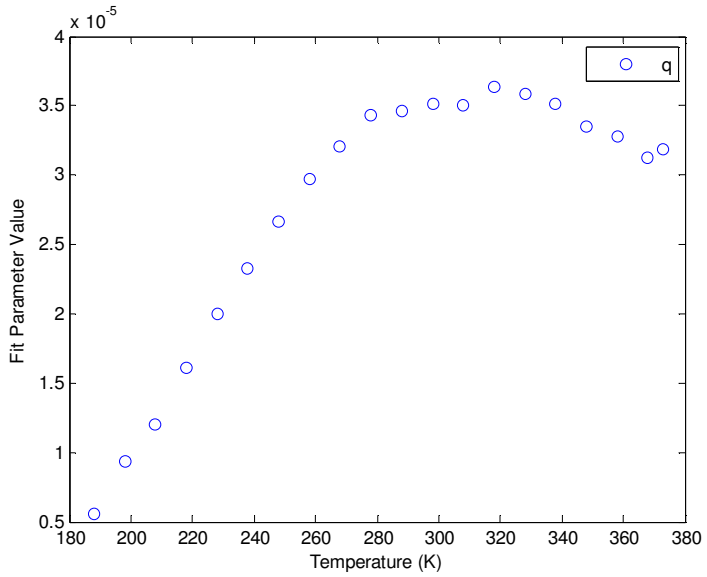

Figure S39. Fit values for the parameter q (Equation S6) for compound **1**.

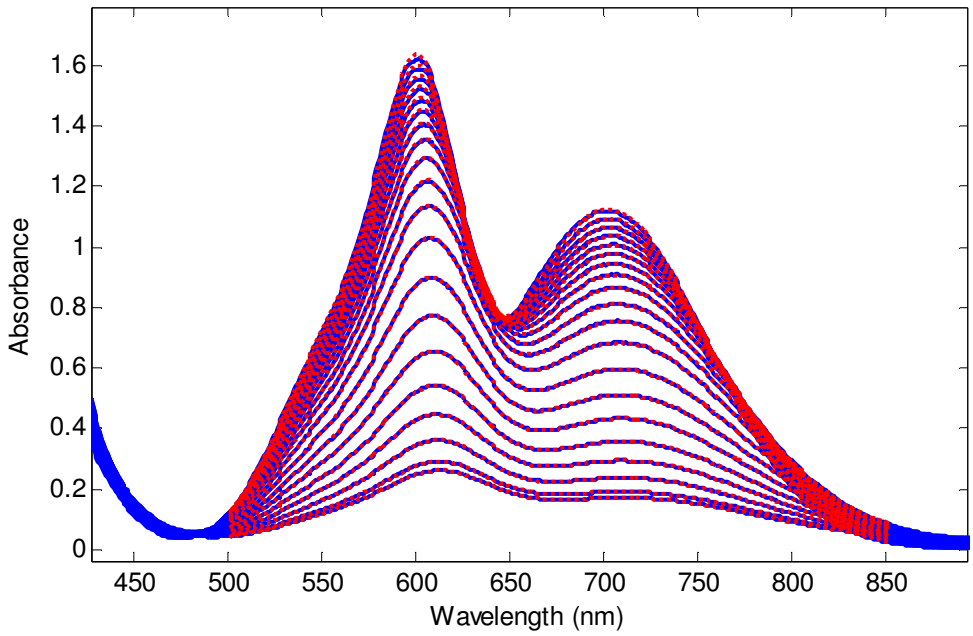

Figure S40. Fits (dotted red lines) according to Equation S6 for the variable-temperature UV-Vis spectra (solid blue lines) of complex **1**.

Parameters l, m, and n, which should be proportional to the concentration of the low-spin form of **1**, were adjusted to account for the change in total concentration of **1** with temperature due to the change in density of toluene.

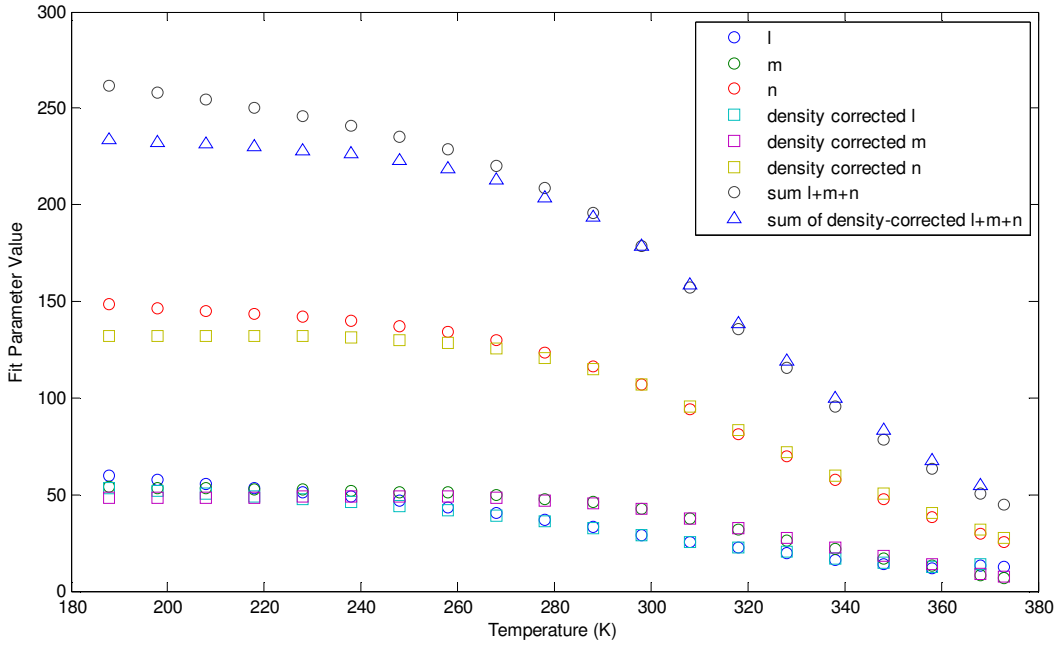

Figure S41. Density correction on fit parameters l, m, and n.

Note that simply plotting the maximum absorbance for a given absorption feature as a function of temperature gives unsatisfactory results (Figure S42) and cannot be well fit to Equation S4 (Figure S43, Table S9), as compared to the results given in Figure 4 (main text) and Table S8.

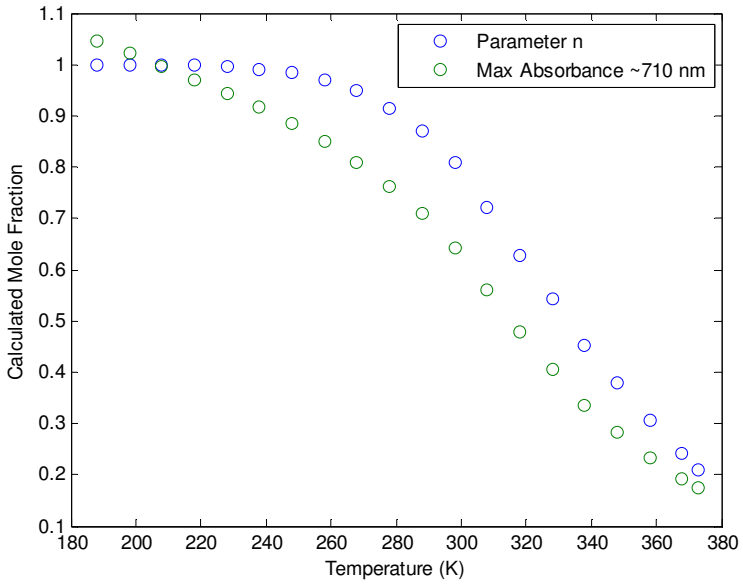

Figure S42. Calculated mole fraction of low-spin form of compound **1** as a function of temperature, calculated (Eqn. S4 and S5, normalized in accordance with the fit to the Boltzmann Equilibrium) based

on either parameter n (area of the 710 nm peak) or the maximum absorbance of the 710 nm peak (after correction for density variations).

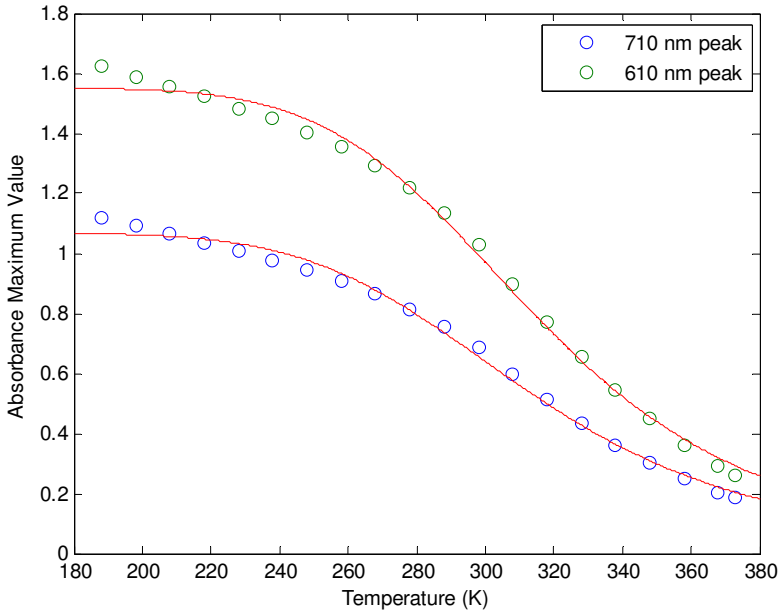

Figure S43. Best fits according to a Boltzmann equilibrium expression for the maximum absorbances of the UV-Vis bands at 710 nm and 610 nm as a function of temperature for compound **1**.

	610 nm peak	710 nm peak
c_{max}	1.551 [1.52, 1.583]	1.068 [1.043, 1.092]
ΔH^o (kJ/mol)	25.0 [22.9, 27.0]	23.4 [21.3, 25.4]
$T_{1/2}$ (K)	316.1 [313.4, 318.9]	313.5 [310.4, 316.6]
Adj. R^2	0.9952	0.9945
RMSE	0.0328	0.0241

Table S9. Fit parameters from the fits shown in Figure S43.

IV. Variable-temperature Mossbauer spectroscopy

A sample of lyophilized **3** was measured across a series of temperatures, and fits to the data were used to probe the Mossbauer parameters and mole fractions of the high- and low-spin states. The lack of measurable change in the low-spin mole fraction between 80 K and 150 K is reflective of the gradual and incomplete solid-state spin-crossover as observed by SQUID magnetometry.

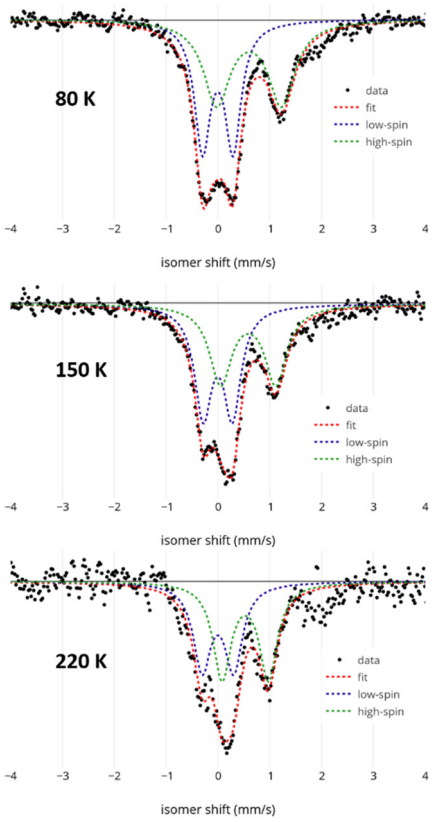

Figure S44. Variable-temperature Mossbauer of lyophilized **3**. A peak discernible around 2 mm/s is likely due to some decomposition of this highly air/water-sensitive sample during handling and measurement.

	isomer shift (δ, mm/s)	quadrupole splitting (ΔE_Q, mm/s)	% composition
3 (lyophilized, 80 K)	0.000	0.603	51
--	0.607	1.252	49
3 (lyophilized, 150 K)	0.000	0.568	51
--	0.584	1.052	49
3 (lyophilized, 220 K)	-0.054	0.612	41
--	0.511	0.919	59

Table S10. Fits to variable-temperature Mossbauer spectra shown in Fig. S44.

IV. Additional SQUID magnetometry data

A complicating effect in the solid-state magnetometry is that the samples appear to undergo an irreversible change in the spin-transition properties upon heating to 400 K. This is apparent in Figure S45 which shows the magnetic moment curves upon heating the sample from 4 K to 400 K and then back. After the first heating cycle no further change is seen regardless of how many times the sample is heated back to 400 K. This does not appear to be due to sample decomposition; NMR analysis of a sample after measurement shows minimal change, and independent experiments confirm that the complexes are thermally stable towards heating to 400 K for several hours in the solid state. Instead, it is likely due to loss of co-crystallized solvent during heating under vacuum, and/or to some other irreversible change in the crystal lattice. This would likely result in decreased crystallinity or more defect-ridden crystals with a higher concentration of grain boundaries, which would be expected to lead to a more gradual and incomplete spin transition, as is observed.[3] If the sample is heated to 400 K under vacuum for several hours *prior* to measurement in the SQUID magnetometer, this change is no longer observed and the initial heating and cooling curves are identical (Figure S46).

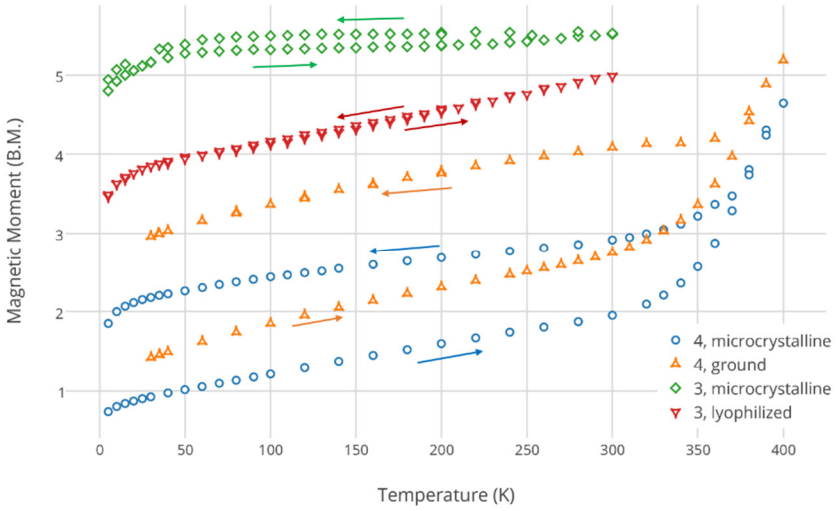

Figure S45. Solid-state magnetometry showing the effect of sample preparation on the measured properties. Arrows show the direction of temperature change for the accompanying trace.

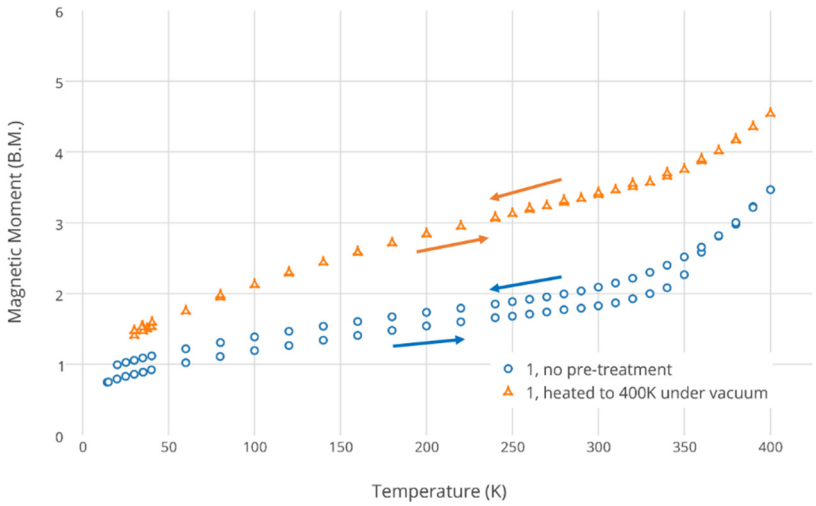

Figure S46. Effect of high-temperature annealing on the observed solid-state magnetic moment of compound **1**. Arrows show the direction of temperature change for the accompanying trace.

V. Crystallographic Details

	1	2	4	5
Crystal system	Triclinic	Triclinic	Monoclinic	Monoclinic
Crystal size (mm)	0.13 x 0.30 x 0.44	0.10 x 0.15 x 0.15	0.20 x 0.28 x 0.31	0.29 x 0.38 x 0.44
Formula	$C_{67.5}H_{55.25}BFeNO_{0.5}P_4$	$C_{72.5}H_{74}BFeNO_{1.5}P_4$	$C_{80.25}H_{146}BFeNP_4$	$C_{141}H_{110}BFeNP_4$
Formula Weight (g/mol)	1078.91	1073.86	1315.51	2008.83
Space group	P-1	P-1	P21/c	P21/n
a (Å)	14.1262(16)	13.4315(6)	26.3693(16)	19.044(4)
b (Å)	14.4698(16)	13.7422(6)	21.5683(16)	26.976(5)
c (Å)	29.339(3)	19.4813(9)	27.7869(19)	21.047(4)
α (deg)	93.996(2)	102.539(2)	90	90
β (deg)	97.983(2)	90.247(2)	92.170(2)	91.667(5)
γ (deg)	105.183(2)	116.120(1)	90	90
Z	2	2	2	4
V ($Å^3$)	5613.8(11)	3131.1(2)	15792.2(19)	10808(4)
Indep. Reflections	26580	19113	71324	35272
R(int)	0.054	0.043	0.112	0.096
R1	0.0588	0.0517	0.0582	0.0745
wR2	0.1703	0.1545	0.1654	0.1873
GOF	1.04	1.05	0.92	1.20

Table S11. Crystallographic details for compounds **1**, **2**, **4**, and **5**.

Compound 1. This compound crystallizes with two independent molecules per asymmetric unit as well as two solvent sites per asymmetric unit. Both solvent sites were modeled as disordered between a THF and a pentane molecule (48:52 and 74:26). Hydrogen atoms were not modeled on the disordered solvents. Additionally, five ligand phenyl rings were modeled as disordered between two positions in 63:47, 70:30, 22:78, and 65:35 ratios. ISOR and SAME restraints as well as EADP constraints where appropriate were used to aid in modeling these disorders. Phenyl rings were restrained with the AFIX 66 command.

Compound 2. This compound crystallizes with two THF solvent sites in the asymmetric unit; one of these sites was modeled as disordered over two positions (76:24). Hydrogen atoms were not modeled on the solvent. Additionally, two of the cyclohexyl rings in the PCy_3 moiety were modeled as disordered over two positions (47:53 and 39:61). ISOR and SAME restraints were used to aid in modeling the disorders.

Compound 4. This compound crystallizes with two independent molecules per asymmetric unit as well as five pentane solvent sites. One pentane site is disordered about a special position (this molecule was modeled without hydrogens) and two others are modeled as disordered over two positions (55:45 ratios); additionally, one cyclohexyl ring from a PCy_3 moiety was modeled as disordered over two positions (45:55). SAME restraints were used to aid in modeling disorders.

Compound 5. This compound crystallizes with one benzene molecule in the asymmetric unit.

	7	**8**	**9**
Crystal system	Orthorhombic	Cubic	Triclinic
Crystal size (mm)	0.19 x 0.30 x 0.32	0.40 x 0.50 x 0.60	0.08 x 0.14 x 0.20
Formula	$C_{45}H_{68}BFeNOP_4$	$C_{45}H_{86}BFeNP_4$	$C_{33}H_{68}BFeNP_4$
Formula weight (g/mol)	813.54	831.68	669.42
Space group	P212121	P213	P-1
a (Å)	10.339(4)	16.8490(5)	10.5753(3)
b (Å)	14.733(5)	16.8490(5)	12.4643(3)
c (Å)	29.561(13)	16.8490(5)	14.9052(4)
α (deg)	90	90	88.155(1)
β (deg)	90	90	79.993(1)
γ (deg)	90	90	89.882(1)
Z	4	4	2
V ($Å^3$)	4503(3)	4783.2(4)	1933.80(9)
Indep. Reflections	21240	8421	12083
R(int)	0.097	0.054	0.032
R1	0.0682	0.0529	0.0427
wR2	0.1607	0.1351	0.1243
GOF	1.06	0.94	1.12

Table S12. Crystallographic details for compounds **7**-**9**.

Compound 7. This complex was modeled with one disordered isopropyl group over two positions (48:52). It was refined as a racemic twin with BASF = 0.01744.

Compound 8. This complex crystallizes on a 3-fold symmetry axis which is collinear with the B-Fe-P(phosphiniminato) axis. The P(*i*Pr)$_2$ and P-Cy moieties were each modeled as disordered over two positions (56:44 and 38:62, respectively) and the B-Ph moiety was modeled as disordered about the three-fold special position.

Compound 9. This complex was refined with two disordered ethyl groups (80:20 and 57:43). ISOR restraints were used to aid in modeling this disorder.

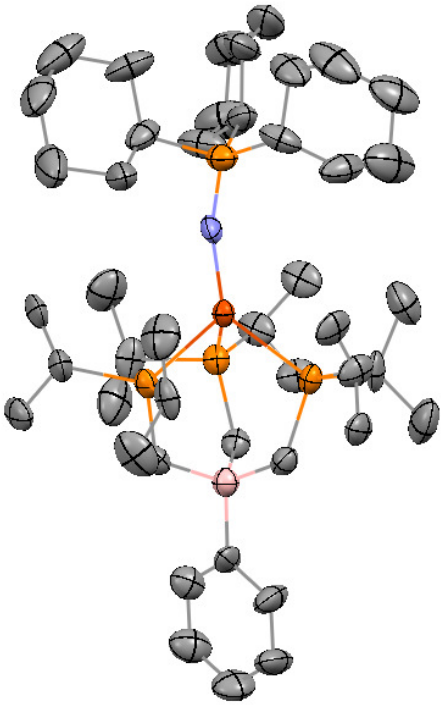

Figure S47. Crystal structure of complex **8**. For clarity, hydrogen atoms are omitted and only one component of disordered groups is shown. The molecule lies on a three-fold axis of symmetry with only one third of the molecule present in the asymmetric unit and the rest generated by symmetry. Thermal ellipsoids are shown at 50%.

VI. Computational Results

A time-dependent DFT calculations was carried out with Gaussian 09 on complex **4** (S = 0) using the crystallographically determined atomic coordinates, and the hybrid B3LYP functional. The 6-311G(df) basis set was used for the iron and phosphorus atoms and 6-31G(d) was used on the remaining atoms. Only the first three singlet excited states were calculated. Although the results are not quantitatively consistent with the measured spectra (this would likely require the use of more sophisticated functional and basis set), they do suggest that the absorbance features absorbed in the visible region do correspond primarily to d-d transitions. The orbitals involved are depicted pictorially in Figure 12 in the main text.

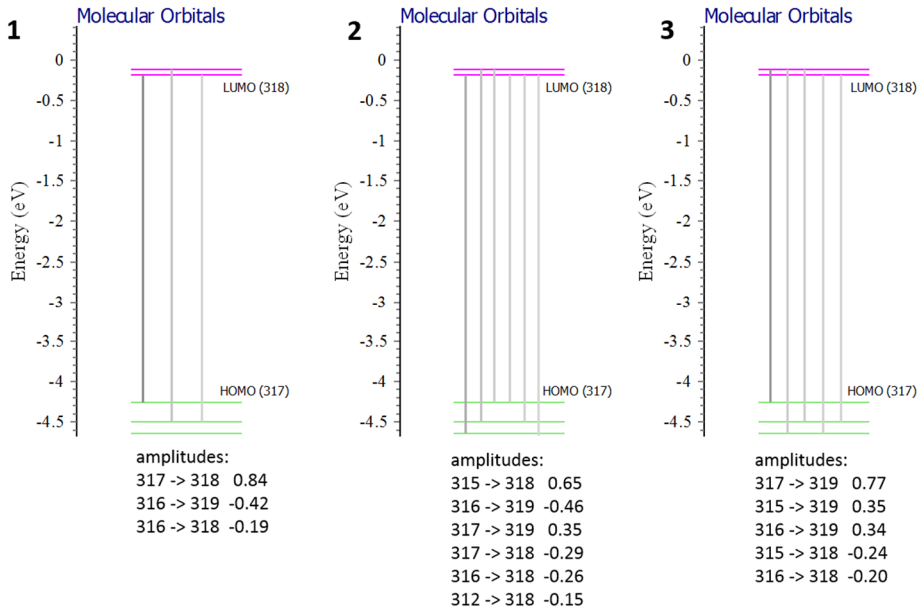

Figure S48. TDDFT results: orbital compositions of the first three calculated singlet excitations.

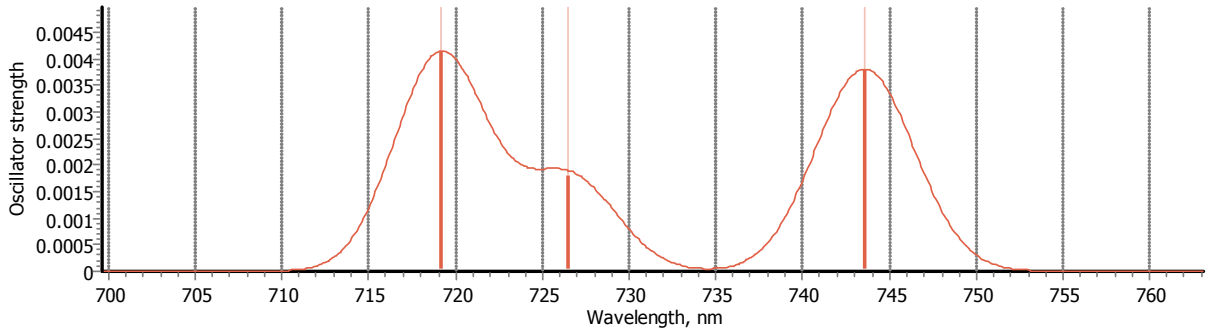

Figure S49. Calculated spectrum (first three singlet excitations).

References

(1) McLinden, M. O.; Splett, J. D. *J. Res. Natl. Inst. Stand. Technol.* **2008**, *113*, 29-67.
(2) Schenker, S.; Hauser, A.; Dyson, R. M. *Inorg. Chem.* **1996**, *35*, 4676-4682.
(3) Salmon, L.; Molnar, G.; Cobo, S.; Oulie, P.; Etienne, M.; Mahfoud, T.; Demont, P.; Eguchi, A.; Watanabe, H.; Tanaka, K.; Bouseksou, A. *New J. Chem.* **2009**, *33*, 1283-1289.